

# 1 **Proprioceptive limit detectors mediate sensorimotor control of the *Drosophila* leg**

2 Brandon G. Pratt<sup>1,2</sup>, Chris J. Dallmann<sup>1,3</sup>, Grant M. Chou<sup>1</sup>, Igor Siwanowicz<sup>4</sup>, Sarah Walling-Bell<sup>1,5</sup>, Andrew  
3 Cook<sup>1</sup>, Anne Sustar<sup>1</sup>, Anthony Azevedo<sup>1</sup>, and John C. Tuthill<sup>1\*</sup>

4  
5 <sup>1</sup>Department of Neurobiology and Biophysics, University of Washington, Seattle, WA, USA

6 <sup>2</sup>Allen Institute for Neural Dynamics, Seattle, WA, USA

7 <sup>3</sup>Neurobiology and Genetics, Julius-Maximilians-University of Würzburg, Würzburg, Germany

8 <sup>4</sup>Janelia Research Campus, Howard Hughes Medical Institute, Ashburn, VA, USA

9 <sup>5</sup>Allen Institute for Brain Science, Seattle, WA, USA

10 \*Lead contact, correspondence to [tuthill@uw.edu](mailto:tuthill@uw.edu)

## 11 12 **Abstract**

13  
14 Many animals possess mechanosensory neurons that fire when a limb nears the limit of its physical range, but the function  
15 of these proprioceptive limit detectors remains poorly understood. Here, we investigate a class of proprioceptors on the  
16 *Drosophila* leg called hair plates. Using calcium imaging in behaving flies, we find that a hair plate on the fly coxa  
17 (CxHP8) detects the limits of anterior leg movement. Reconstructing CxHP8 axons in the connectome, we found that they  
18 are wired to excite posterior leg movement and inhibit anterior leg movement. Consistent with this connectivity,  
19 optogenetic activation of CxHP8 neurons elicited posterior postural reflexes, while silencing altered the swing-to-stance  
20 transition during walking. Finally, we use comprehensive reconstruction of peripheral morphology and downstream  
21 connectivity to predict the function of other hair plates distributed across the fly leg. Our results suggest that each hair  
22 plate is specialized to control specific sensorimotor reflexes that are matched to the joint limit it detects. They also illustrate  
23 the feasibility of predicting sensorimotor reflexes from a connectome with identified proprioceptive inputs and motor  
24 outputs.

## 25 26 **Introduction**

27  
28 Animals rely on proprioception to sense and coordinate movements of the body. One key function of the proprioceptive  
29 system is to detect when a body part has reached the limits of its normal range. In vertebrates, including mammals, the  
30 extremes of joint position are detected by low-threshold Ruffini endings and Pacinian corpuscles embedded within joint  
31 capsules (Burgess and Clark, 1969). In arthropods, including insects, joint limits may be detected by hair plates, fields of  
32 small, stiff mechanosensory hairs positioned at cuticular folds within joints (Pringle, 1938). Compared to proprioceptors  
33 that encode limb position and movement, such as vertebrate muscle spindles and invertebrate chordotonal organs, less is  
34 known about the physiology and behavioral function of proprioceptors that detect joint limits (Tuthill and Azim, 2018).

35 Early recordings from joint receptors in cats found that single afferents fired in a phasic or tonic manner near the limit of  
36 the range of joint movement (Burgess and Clark, 1969). For much of the 20<sup>th</sup> century, it was believed that these receptors  
37 were the primary source of our conscious sense of body position, or kinesthesia (Proske and Gandevia, 2012). However,  
38 humans retain their kinesthetic sense after joint capsules are removed following hip replacement surgery (Grigg et al.,  
39 1973). This and other evidence (Clark et al., 1979) suggests that muscle spindles are the primary proprioceptors underlying  
40 kinesthesia in mammals. Although joint receptors may not be required for kinesthesia, they could still play a role in  
41 unconscious, reflexive control of movement, a hypothesis which has received less attention since the focus shifted to  
42 muscle spindles (Proske and Gandevia, 2012).

43 In insects and other invertebrates, feedback from proprioceptive limit detectors has been shown to initiate stabilizing  
44 reflexes that sculpt motor patterns and protect the limbs from injury (Bässler, 1977). For example, classic work in the  
45 cockroach showed that hair plate neurons at a proximal leg joint monosynaptically excite extensor motor neurons and  
46 indirectly inhibit flexor motor neurons, restricting the range of joint flexion (Pearson et al., 1976; Wong and Pearson,  
47 1976). The ablation of this hair plate caused the corresponding leg to overstep and collide with the more anterior leg  
48 during walking, indicating that limit detection is important for controlling phase transitions of the step cycle (Wong and  
49 Pearson, 1976). Past work has identified specific sensorimotor reflexes mediated by insect hair plates, but it has been  
50 difficult to synthesize into a more comprehensive understanding of the underlying feedback circuits and their function.  
51 Like many proprioceptors, hair plates are distributed throughout the animal's body, which raises the possibility that each  
52 sensory organ is specialized for sensing and controlling specific movements.

53 With emerging connectomic wiring maps (Azevedo et al., 2024; Dorckenwald et al., 2024; Takemura et al., 2024; Winding  
54 et al., 2022) and genetic tools to target specific cell types (Jenett et al., 2012), the fruit fly, *Drosophila*, has recently  
55 emerged as an important model system to investigate neural mechanisms of limb proprioception. We and others have used  
56 connectomics (Lee et al., 2024; Marin et al., 2024), electrophysiology (Agrawal et al., 2020), calcium imaging (Chen et  
57 al., 2021; Dallmann et al., 2023; Mamiya et al., 2023, 2018), and behavior (Akitake et al., 2015; Cheng et al., 2010;  
58 Chockley et al., 2022; Isakov et al., 2016; Mendes et al., 2013; Pratt et al., 2024), to investigate the function of  
59 proprioceptors in the fly's femoral chordotonal organ (FeCO). The FeCO contains subtypes of mechanosensory neurons  
60 that detect the position, movement, and vibration of the fly femur-tibia joint, in a manner analogous to vertebrate muscle  
61 spindles (Mamiya et al., 2023, 2018). However, compared to the FeCO, little is currently known about the anatomy,  
62 physiology, and behavioral function of hair plates on the *Drosophila* leg.

63 The six *Drosophila* legs have 214 hair plate mechanosensory neurons that are clustered into 42 hair plates (**Figure S1A**)  
64 (Hodgkin and Bryant, 1979; Kuan et al., 2020; Schubiger, 1968). Investigating the physiology and function of each hair  
65 plate, one-by-one, would be experimentally intractable, even in the tiny fruit fly. Instead, we start by studying one specific  
66 hair plate on the coxa of the fly's front legs (CxHP8) using *in vivo* calcium imaging (**Figure 1**), connectomics (**Figure 2**),  
67 and genetic manipulations during behavior (**Figures 3, 4**). We find that the sensory tuning and motor reflex action of  
68 CxHP8 are well predicted by its external morphology and downstream connectivity to leg motor neurons. We therefore  
69 extend these sensorimotor reflex predictions to other hair plates positioned at different locations on the leg (**Figure 5**).  
70 Overall, our results provide insight into the behavioral function of proprioceptive limit detectors and illustrate a new  
71 approach for comprehensive analysis of distributed sensorimotor systems that can be scaled to other animals.

72

## 73 **Results**

74

### 75 **CxHP8 neurons detect the limits of coxa rotation and adduction**

76

77 On the fly's front leg, three hair plates are located at the junction between the coxa (Cx) and thorax (**Figure 1A**). These  
78 hair plates (CxHP8, CxHP3, CxHP4) wrap the joint along the anterior-posterior axis. We screened Split-GAL4 driver  
79 lines to identify lines that label coxa hair plates (**Table S1**). The most specific and complete line we found (Oh et al.,  
80 2021) labeled CxHP8 neurons on the front and middle legs (6 and 3 out of 8 cells, respectively). Using this specific driver  
81 line, which we refer to as CxHP8-GAL4 (**Figure 1B; Figure S1B**), we first investigated the joint angle encoding  
82 properties of CxHP8 neurons.

83 We used a previously described setup (Dallmann et al., 2023) that combines 2-photon calcium imaging with high-speed  
84 video to simultaneously record the activity of CxHP8 axons and 3D leg joint kinematics in CxHP8-GAL4 flies expressing  
85 GCaMP7f and tdTomato (**Figure 1C**). To overcome the slow temporal dynamics of GCaMP7f relative to the dynamics  
86 of active leg movement in flies, we passively (and slowly) moved the left front leg using a manually controlled 3-axis

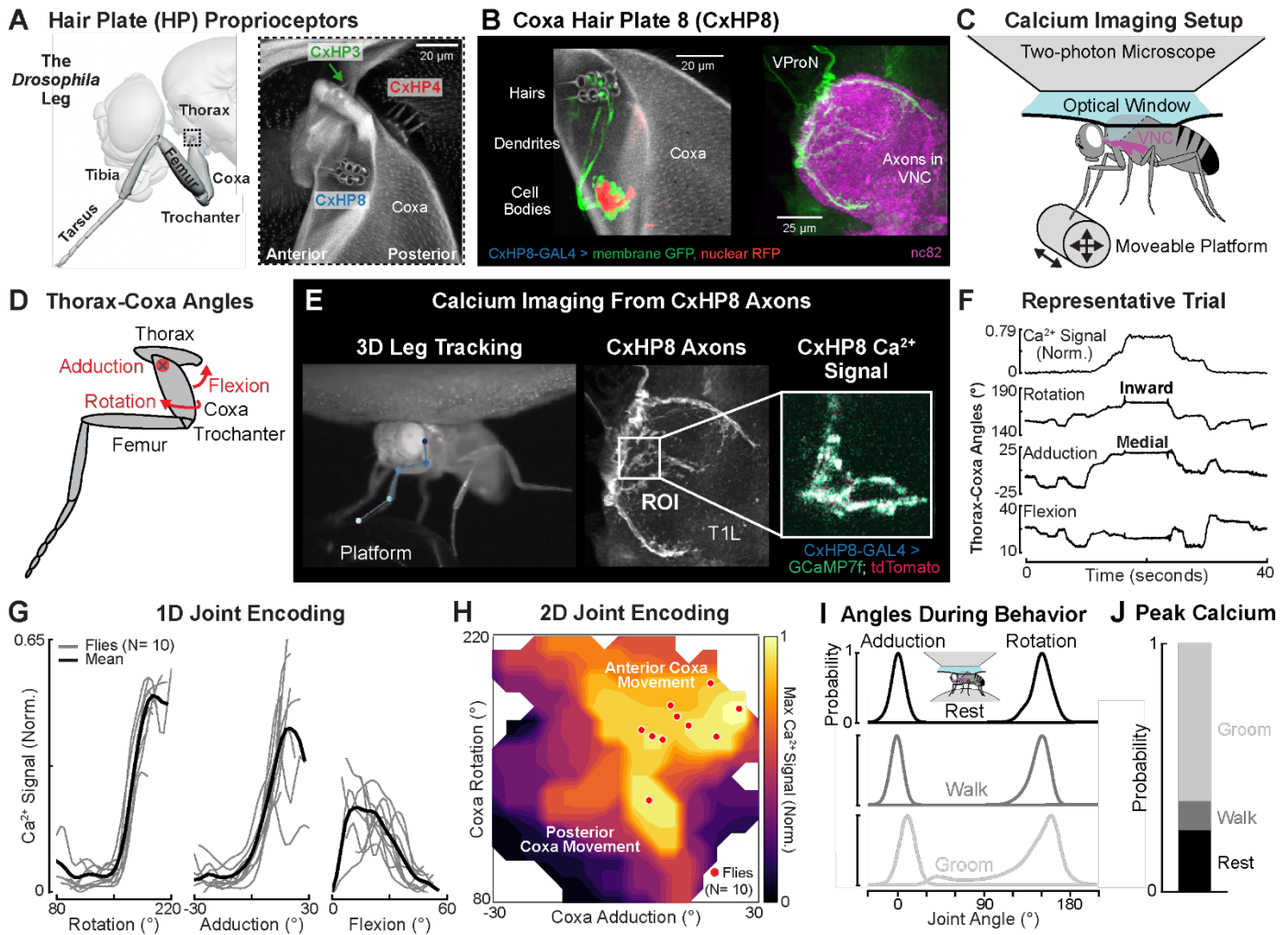
87 platform (**Video 1**). We then used DeepLabCut (Mathis et al., 2018) and Anipose (Karashchuk et al., 2021) to compute  
88 the 3 angles corresponding to the rotation, adduction, and flexion of the front leg thorax-coxa joint (**Figure 1D**). Increases  
89 in rotation, adduction, and flexion angles correspond to the coxa rotating inward, translating medially, and flexing,  
90 respectively (**Figure S1C**). Our goal in these experiments was to determine the relationship between thorax-coxa joint  
91 angles and CxHP8 calcium activity (**Figure 1E**).

92 Based on the anterior position of CxHP8 at the thorax-coxa joint, we hypothesized that its hairs would be deflected during  
93 anterior and medial movements, and inward rotations of the coxa (**Video 2**). A representative trial indeed shows a peak  
94 calcium signal when the coxa was inwardly rotated and adducted (**Figure 1F**). Across flies, we found similar tuning to  
95 coxa rotation and adduction (**Figure 1G**). Although with more variability, CxHP8 axons showed higher activity when the  
96 coxa was extended. Because coxa rotation and adduction produced strong calcium responses, we next investigated how  
97 the two angles jointly influenced the activity of CxHP8 neurons. We found that the combination of both adduction and  
98 inward rotation resulted in maximal calcium activity of CxHP8 axons (**Figure 1H**). Altogether, our results show that  
99 CxHP8 neurons detect the limits of anterior leg movement.

## 100 **CxHP8 neurons are active across behaviors**

101

102 We next sought to determine which behaviors were accompanied by the extreme anterior coxa movements that drive  
103 CxHP8 activity. We used a similar imaging setup (Dallmann et al., 2023) but replaced the platform with an air-supported  
104 ball and allowed the fly to spontaneously behave (**Video 3**). We found that resting, walking, and grooming produced  
105 rotation and adduction coxa joint angles within the range that CxHP8 neurons were active (**Figure 1I**). As illustrated by  
106 a representative trace, calcium activity increased during grooming and walking compared to adjacent resting states  
107 (**Figure S1D**). Peak calcium activity was largest for front leg grooming bouts, likely because of the sustained deflection  
108 of CxHP8 cuticular hairs. Thresholding peak calcium activity (**Figure 1E**), we found CxHP8 neurons were active across  
109 behaviors (**Figure 1J**), particularly during extreme adduction and rotation angles (**Figure S1F**).



110  
111  
112 **Figure 1. CxHP8 neurons encode the anterior limits of thorax-coxa joint angles.** (A) Left: schematic rendering of the fly's front leg. Right: a  
113 confocal image of the three hair plates, CxHP3, CxHP4, and CxHP8, at the thorax-coxa joint (black dotted box) of the front leg. (B) Confocal images  
114 of genetically labeled CxHP8 neurons (6 of 8) in the coxa of the front leg and ventral nerve cord (VNC). CxHP8 (autofluorescence: gray) consists  
115 of 8 cuticular hairs located on the coxa. Each hair is innervated by a single mechanosensory neuron (GFP: green), which projects through the ventral  
116 prothoracic nerve (VProN) into the VNC (nc82: magenta). The cell bodies of CxHP8 neurons are labeled in red (redstinger). (C) Schematic of the  
117 setup used to measure calcium signals from CxHP8 axons as the left front leg was passively moved on a platform. (D) Schematic of the rotation,  
118 adduction, and flexion thorax-coxa joint angles. (E) Example recording of calcium activity of CxHP8 axons. Joint angles were quantified by tracking  
119 the joints of the left front leg in 3D. In addition to GCaMP7f (green), CxHP8 axons expressed tdTomato (red) for motion correction and signal  
120 normalization. (F) Representative trial showing the normalized calcium signal for CxHP8 axons, the thorax-coxa rotation, adduction, and flexion  
121 angles while the left front leg was passively moved. Calcium activity was normalized between 0 and 1, where 1 represents the greatest calcium  
122 activity in the dataset. (G) Normalized calcium activity of CxHP8 axons with respect to thorax-coxa rotation, adduction, and flexion angles. Black  
123 line: bin averaged mean calcium activity across all flies; Gray lines: bin averaged mean calcium activity for each fly. (H) Contour plot showing the  
124 maximum 2D calcium activity across all flies with respect to thorax-coxa rotation and adduction. Red dots: the rotation and adduction angles at  
125 which the normalized calcium activity was maximum for each fly. (I) Adduction and rotation joint angle normalized probability densities across  
126 flies during rest (black), walking (gray), and front leg grooming (light gray). The inset shows a schematic of the calcium imaging setup used to  
127 determine CxHP8 activity during behavior. (J) Probability of flies grooming, walking, or resting during peak calcium activity. See also **Figure S1**  
128 **and Videos 1-3.**

129  
130  
131  
132  
133

## 134 **Connectomics predict that CxHP8 neurons drive posterior leg movement**

135

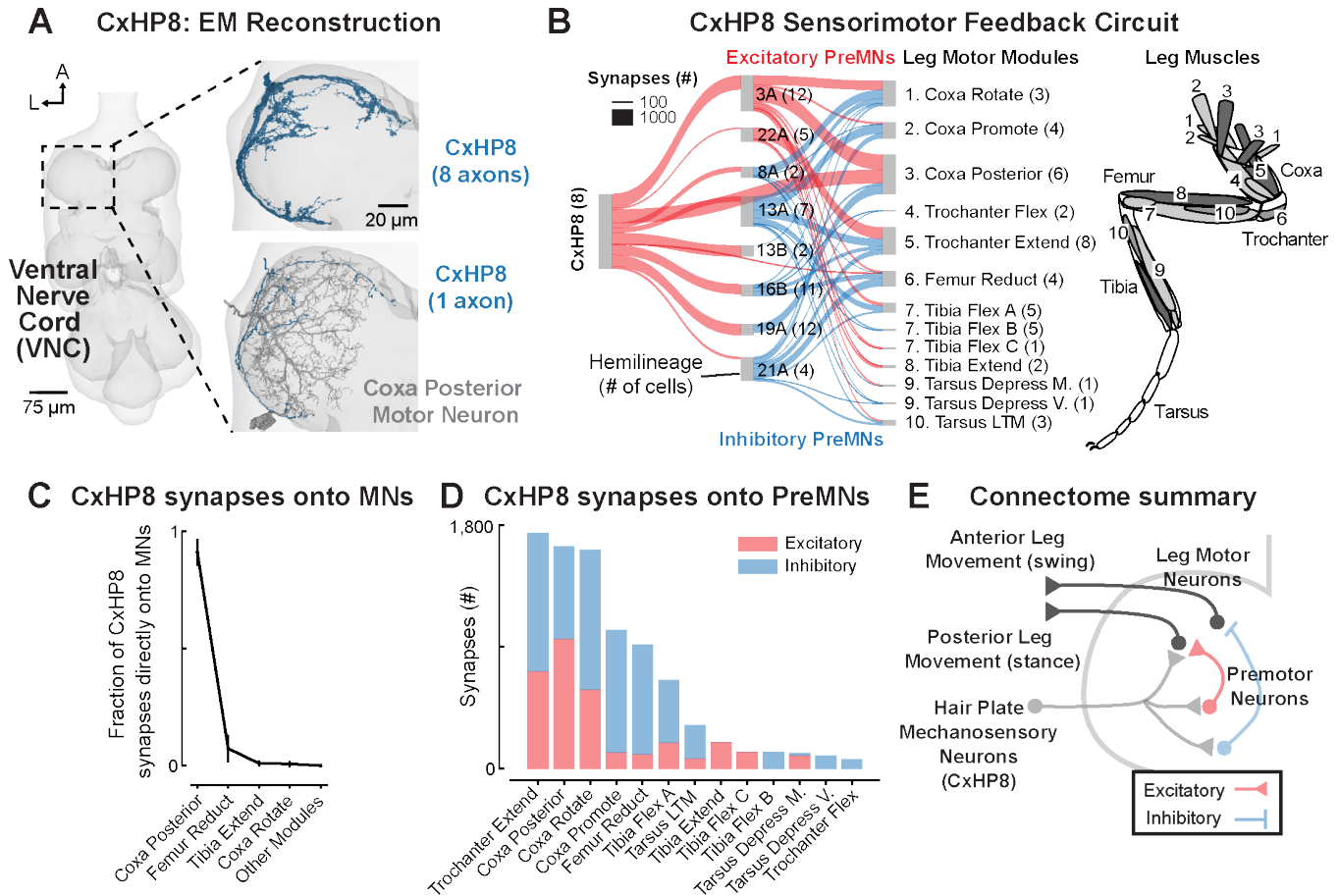
136 Using connectomics, we next reconstructed and analyzed hair plate sensorimotor circuits to predict the role of limit  
137 detection in leg motor control. Some hair plate axons were previously reconstructed in an electron microscopy (EM)  
138 dataset of a male adult nerve cord (MANC) (Marin et al., 2024). However, specific hair plate axons could not be identified  
139 in MANC due to poor reconstruction quality. We therefore reconstructed hair plate axons within an EM dataset of the  
140 Female Adult Nerve Cord (FANC)(Azevedo et al., 2024; Phelps et al., 2021). We first used previous annotations (Phelps  
141 et al., 2021) to identify and proofread all CxHP8 axons projecting into the left leg neuromere (**Figure 2A**). We identified  
142 the peripheral location of each hair plate axon in the FANC connectome using a combination of genetic driver lines,  
143 axonal morphology, axonal projection patterns, and an x-ray holographic nano-tomography dataset of the fly leg (Kuan  
144 et al., 2020) (See Methods for details). For example, CxHP8 cells are identifiable in the X-ray dataset because they are  
145 the only hair plate axons that project into the VNC through the ventral prothoracic nerve (VProN).

146

147 The entire FANC dataset has been automatically segmented into neurons using convolutional neural networks (Azevedo  
148 et al., 2024), but many cells still required manual proofreading. We proofread and annotated cells downstream of CxHP8  
149 neurons and found that CxHP8 axons allocate 75% of their output synapses ( $2,279 \pm 482$  synapses per CxHP8 axon) to  
150 premotor (interneurons that synapse on motor neurons: 58%) and motor (17%) neurons. This percentage is significantly  
151 higher than that of exteroceptive leg sensory neurons, but similar to FeCO proprioceptors (Lee et al., 2024), suggesting  
152 that hair plates are primarily involved in leg motor control.

153

154 The 69 motor neurons controlling the fly's left front leg are organized into 14 motor modules – motor neurons within a  
155 module receive common presynaptic input and control the same joint (Azevedo et al., 2024). Premotor neurons in FANC  
156 have also been annotated based on their developmental hemilineage (Lesser et al., 2024), from which it is possible to infer  
157 the neurotransmitter released by each cell (acetylcholine, GABA, or glutamate). We first examined the connectivity from  
158 CxHP8 axons to premotor neurons to leg motor neurons (**Figure 2B**). CxHP8 neurons provide strong monosynaptic input  
159 to motor neurons within the coxa posterior module (**Figure 2B,C**). They also connect indirectly, via excitatory and  
160 inhibitory premotor neurons, to multiple other motor modules across the leg (**Figure 2C, Figure S2A**). CxHP8's strongest  
161 inhibitory connections are onto the coxa promote module, an antagonist of the coxa posterior module (**Figure 2B**). We  
162 also found extensive recurrent connectivity within and across premotor neurons, as well as between CxHP8 axons and  
163 19A premotor neurons (**Figure S2B**). Overall, CxHP8 neurons are positioned to provide feedback to multiple motor  
164 modules, but with the strongest excitation to motor neurons driving posterior leg movement and inhibition to motor  
165 neurons driving anterior movements. These connectivity patterns lead us to hypothesize that activity in CxHP8 neurons  
166 drives posterior leg movement when the coxa reaches its anterior limit. For example, CxHP8 feedback could contribute  
167 to the swing-to-stance transition during walking (**Figure 2E**).



168

169 **Figure 2. Synaptic connectivity suggests that CxHP8 neurons connect to a reflex circuit that drives posterior leg movement.** (A) We  
 170 reconstructed all CxHP8 axons within the left front leg neuromere of a *Drosophila* female VNC (FANC) electron microscopy volume. (B) CxHP8  
 171 axons synapse onto premotor neurons, identified by their hemilineage, as well as motor neurons grouped into motor modules (Azevedo et al., 2024).  
 172 Red and blue lines signify excitatory and inhibitory connections, respectively. The strength of the connection (width of the line) is the number of  
 173 synapses all neurons within a cell class make onto a downstream cell class. Only premotor and motor neurons that received an average of 4 or greater  
 174 synapses per neuron from an upstream cell class were analyzed (i.e., CxHP8 input threshold: 8 cells \* 4 synapses). The number of cells in each cell  
 175 class included in this analysis is indicated within parentheses. The numbers in the leg schematic on the right illustrate the muscles belonging to leg  
 176 motor modules 1-10. (C) CxHP8 neurons primarily synapse onto motor neurons within the coxa posterior motor module. Error bars are standard  
 177 deviation. (D) Relative number of excitatory and inhibitory synapses between premotor neurons that receive input from CxHP8 neurons and motor  
 178 neurons within motor modules. Red and blue bars indicate excitatory and inhibitory connections, respectively. (E) Summary schematic showing the  
 179 circuit through which CxHP8 neurons are predicted to drive posterior leg movement. See also **Figure S2**.

180

181

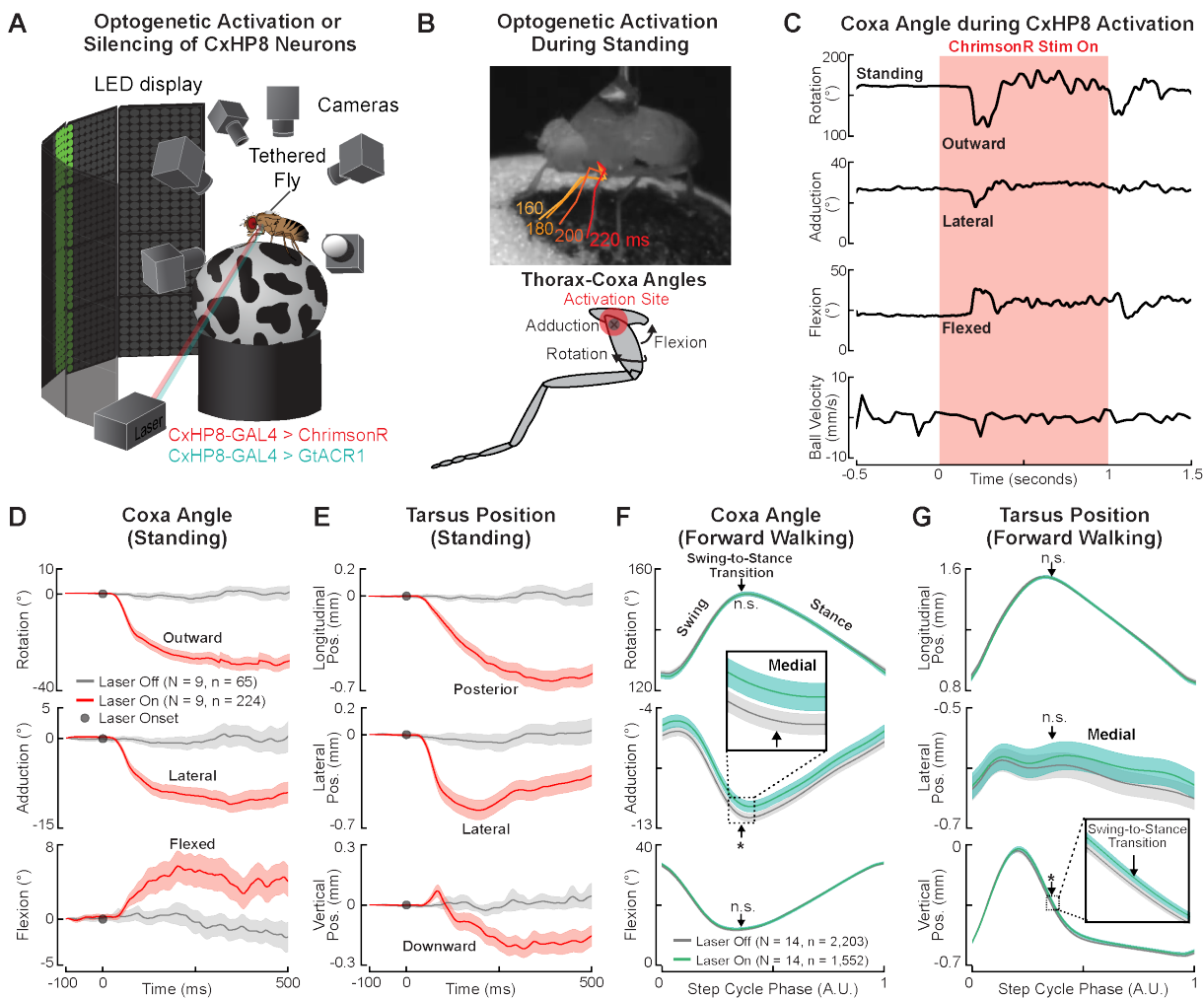
## 182 CxHP8 activation drives posterior leg movement and silencing alters swing-to-stance transitions during walking

183

184 We next tested whether CxHP8 activation contributes to posterior leg movements, as predicted by their synaptic  
 185 connectivity to leg motor neurons. As in prior studies (Agrawal et al., 2020; Azevedo et al., 2020), we used a setup that  
 186 enables spatiotemporally precise optogenetic activation or silencing of neurons in tethered flies behaving on an air-  
 187 supported ball (**Figure 3A**). Using six high-speed cameras, we reconstructed full 3D leg joint kinematics using  
 188 DeepLabCut (Mathis et al., 2018) and Anipose (Karashchuk et al., 2021). To optogenetically activate CxHP8 neurons,  
 189 we genetically expressed ChrimsonR within the CxHP8 neurons and illuminated the thorax-coxa joint of the left front leg  
 190 with a red laser. In a representative standing fly, we observed that its left front leg moved posteriorly shortly after the  
 191 onset of the laser, which was accompanied by outward rotation, lateral movement, and flexion of the coxa (**Figure 3B,C**).  
 192 We observed the same changes in thorax-coxa joint angles across standing flies (**Figure 3D**). These joint angle changes

193 were accompanied by posterior, lateral, and downward displacement of the distal tarsus (**Figure 3E**). Overall, the  
 194 activation of CxHP8 neurons produced posterior and lateral movement of the stimulated leg, without impacting the other  
 195 legs.

196 We next optogenetically silenced CxHP8 neurons through the expression of a light-gated chloride channel (GtACR1)  
 197 during spontaneous behaviors. When CxHP8 feedback was disrupted during forward walking, the thorax-coxa adduction  
 198 angle of the left front leg was slightly but significantly more medial, particularly at the swing-to-stance transition of the  
 199 step cycle (**Figure 3F**). We did not observe medial coxa displacements in control flies that experienced the same laser  
 200 stimulation (**Figure S3A**). Optogenetic silencing of CxHP8 neurons also subtly but significantly altered the tarsus position  
 201 at the swing-to-stance transition (**Figure 3G**). Thus, the lack of CxHP8 activity appeared to cause the coxa to slightly  
 202 overshoot the normal kinematic range associated with the swing-to-stance transition, leading to a medial displacement of  
 203 the entire leg. We also assessed the role of CxHP8 feedback in left (**Figure S3B**) and right turns (**Figure S3C**), and front  
 204 leg grooming (**Figure S3D**). Although joint angles were not affected during left turns, we found that the coxa was  
 205 significantly more extended and rotated inward at the swing-to-stance transition when CxHP8 neurons were silenced  
 206 during right turns. The coxa was also significantly more extended and adducted in flies with CxHP8 neurons silenced  
 207 during front leg grooming.



208

209 **Figure 3. CxHP8 neurons drive posterior leg movement to mediate the swing-to-stance transition during walking.** (A) Schematic of the  
 210 optogenetic activation and silencing setup. 6 high-speed cameras (300 fps) recorded the behavior of a tethered fly on a ball and a laser focused on  
 211 the left front leg was used to excite or inhibit CxHP8 neurons expressing the light-gated ion channel ChrimsonR (red) or GtACR1 (green). Trials  
 212 were 2 s in duration and the laser was presented for 1 s during experimental trials and absent during control trials. (B) Top: example trial in which

213 CxHP8 activation resulted in outward rotation, lateral movement, and flexion of the coxa in a standing fly. The amount of time, in ms, passed after  
214 the onset of the laser is displayed in the same color as the corresponding skeletonized leg. Bottom: the rotation, adduction, and flexion thorax-coxa  
215 joint angles. (C) For the same trial shown in B, the thorax-coxa rotation, adduction, and flexion angles, and the ball velocity in response to the  
216 optogenetic activation of CxHP8 neurons. (D) Optogenetic activation (red) of CxHP8 neurons in standing flies resulted in significant outward  
217 rotation, lateral displacement, and flexion of the coxa compared to trials in which the laser remained off (gray). Shaded region: 95% confidence  
218 interval; N: number of flies; n: number of trials. (E) Optogenetic activation (red) of CxHP8 neurons in standing flies also resulted in significant  
219 lateral and posterior movements of the tarsus compared to trials in which the laser remained off. The tarsus also moved downward along the ball  
220 during optogenetic activation. Shaded region: 95% confidence interval; N: number of flies; n: number of trials. (F) Optogenetic silencing (green) of  
221 CxHP8 neurons in flies walking forward produced a significant (\*:  $p < 0.025$ ) medial movement of the coxa near the swing-to-stance transition  
222 compared to forward walking steps when the laser was off (gray). Arrow: the average swing-to-stance transition of the step cycle; Shaded region:  
223 95% confidence interval; N: number of flies; n: number of steps. A t-test with a Bonferroni correction of 2 was used to statistically compare the  
224 distributions of joint angles at the swing-to-stance transition. (G) Optogenetic silencing (green) of CxHP8 neurons in flies walking forward also  
225 resulted in a more medial and significantly higher (\*:  $p < 0.025$ ) tarsus position following the swing-to-stance transition compared to forward walking  
226 steps when the laser was off (gray). A t-test with a Bonferroni correction of 2 was used to statistically compare the distributions of tarsus positions  
227 at the swing-to-stance transition. See also **Figure S3**.

228

### 229 **CxHP8 facilitates the swing-to-stance transition and controls resting posture in untethered flies**

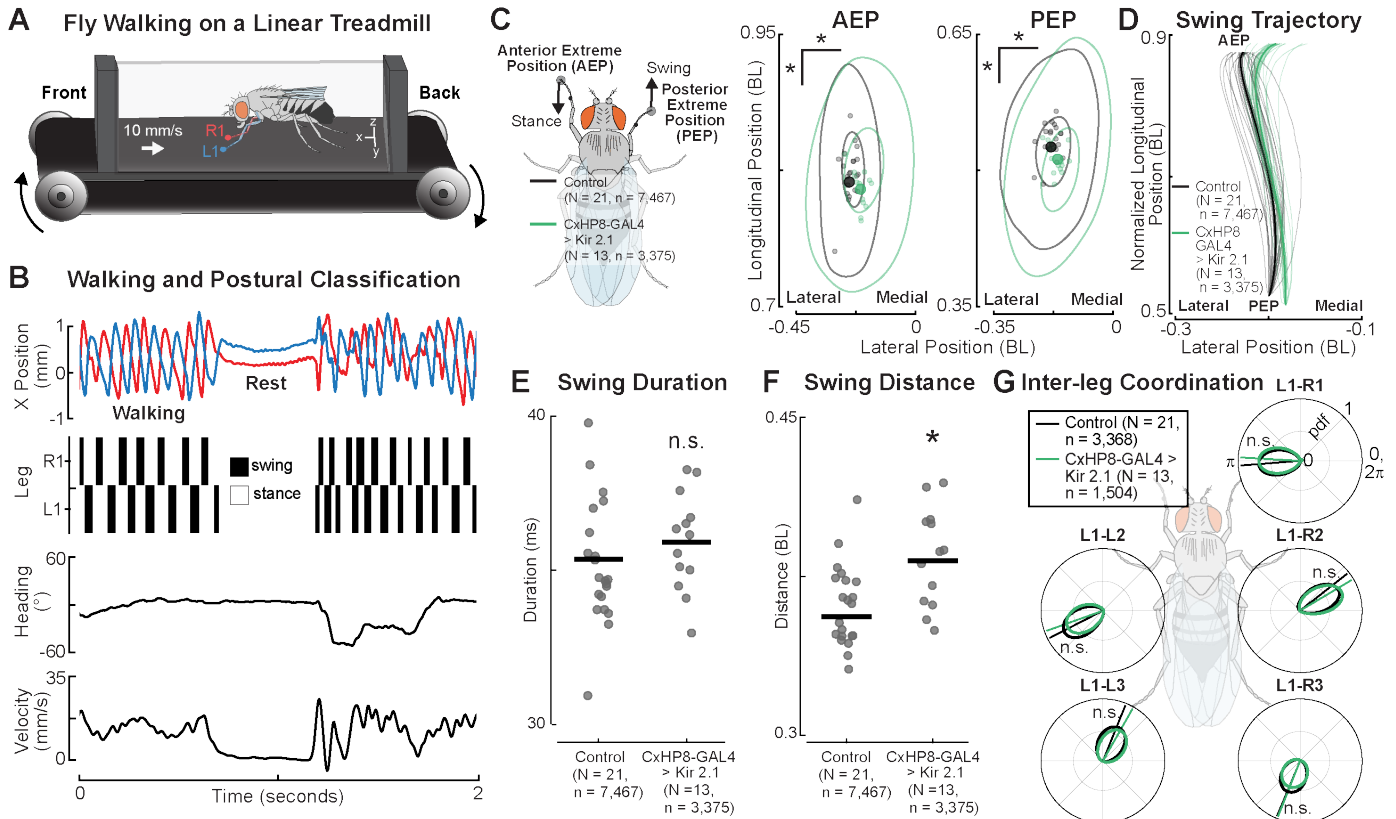
230

231 Although convenient for delivering targeted optogenetic stimuli and tracking joint kinematics, flies walking in the tethered  
232 configuration have slightly different walking kinematics than untethered flies (Pratt et al., 2024). To test whether CxHP8  
233 feedback is important for the control of swing-to-stance transitions in untethered walking flies, we used a linear treadmill  
234 system (Pratt et al., 2024). We genetically expressed an inward rectifying potassium channel, Kir 2.1, to chronically  
235 hyperpolarize CxHP8 neurons. As flies walked on the treadmill, driven at a belt speed of 10 mm/s, we recorded their  
236 movement at 200 fps with 5 high-speed cameras (**Figure 4A**). From the high-speed videos, we reconstructed the 3D  
237 positions of the head, thorax, abdomen, and each leg tip using DeepLabCut (Mathis et al., 2018) and Anipose (Karashchuk  
238 et al., 2021). We then used these reconstructed 3D positions to quantify kinematics and posture during walking and rest  
239 periods, respectively (see Methods for details; **Figure 4B**).

240 Like tethered flies, we also found silencing CxHP8 neurons in flies walking on the treadmill impaired step kinematics of  
241 the front legs near the swing-to-stance transition. In particular, the anterior extreme position (AEP), where a leg first enters  
242 stance, was displaced medially and posteriorly compared to controls (**Figure 4C**). The posterior extreme position (PEP),  
243 where a leg first enters swing, was also significantly displaced in a similar manner to the AEP. Given that the AEP marks  
244 the swing-to-stance transition, and that changes in the AEP may drive changes in the PEP, we focused on understanding  
245 the kinematic changes that facilitate the displacement of the AEP in CxHP8-silenced flies. In examining the average swing  
246 trajectories of the front legs, we found a significant medial deviation of the trajectory near the swing-to-stance transition  
247 in CxHP8 silenced flies compared to controls (**Figure 4D**). Although this deviation did not result from a significantly  
248 longer mean swing duration (**Figure 4E**), the mean swing distance was significantly greater in flies with CxHP8 neurons  
249 silenced (**Figure 4F**). Unlike front leg step kinematics, inter-leg coordination was not significantly altered in flies with  
250 CxHP8 neurons silenced (**Figure 4G**). Overall, the silencing of CxHP8 neurons in flies walking on the treadmill resulted  
251 in more medial front leg movement near the swing-to-stance transition, consistent with our results from tethered flies.

252 In larger insects, hair plates have been shown to be important for controlling resting body (Wendler, G., 1972) and leg  
253 posture (Bässler, 1977; Theunissen et al., 2014). We therefore examined the posture of flies during rest periods on the  
254 treadmill. Even though flies with CxHP8 neurons silenced didn't have significantly different body heights (**Figure S4A**)  
255 or angles (**Figure S4B**), the resting positions of their tarsi were significantly more splayed out than controls (**Figure S4C**).  
256 We further quantified this by calculating the area of the polygon formed by the tarsi positions (**Figure S4D**). The mean  
257 polygon area of CxHP8 silenced flies was significantly greater than controls, providing further support that CxHP8  
258 neurons control the resting posture of the legs.

259



260

261 **Figure 4. CxHP8 neurons control swing-to-stance transitions in unconstrained flies.** (A) Schematic of the treadmill system. Flies were recorded  
 262 with 5 high-speed cameras (200 fps) as they walked on a treadmill with a belt speed of 10 mm/s. The 3D positions of each distal leg tip and the head,  
 263 thorax, and abdomen were tracked using automated pose estimation methods. (B) Example trial period illustrating that both walking kinematics and  
 264 resting posture can be obtained using the treadmill system. Shown are the longitudinal (X) position and the classification of swing and stance of the  
 265 left and right front leg as the fly walked and rested on the treadmill belt. Walking and rest periods were classified using the heading and body velocity  
 266 of the fly. (C) Left: Schematic of the anterior and posterior extreme positions. Right: Kernel density estimation plots of the anterior and posterior  
 267 extreme positions significantly shifted medially and posteriorly in flies with CxHP8 neurons chronically silenced (green) with the inward rectifying  
 268 potassium channel, Kir 2.1. N: number of flies; n: number of steps. Bootstrapping with a Bonferroni correction of 12 was used to statistically compare  
 269 CxHP8 silenced and control flies (\*:  $p < 0.004$ ). (D) Swing trajectories of CxHP8 silenced (green) and control (black) flies demonstrate the medial  
 270 overshoot near the swing-to-stance transition when CxHP8 neurons were silenced. Each trajectory was scaled by the average swing distance and  
 271 began at the average posterior extreme position. Solid line: mean trajectory; Thin lines: mean trajectory of each fly; Shaded region: 95% confidence  
 272 interval; N: number of flies; n: number of steps. (E) Swing duration was not statistically different between CxHP8 silenced and control flies,  
 273 based on a t-test with a Bonferroni correction of 2 on the means of flies (n.s.:  $p > 0.025$ ). (F) Swing distance was significantly greater for CxHP8 silenced  
 274 flies compared to controls (\*:  $p < 0.025$ ). (G) Inter-leg coordination (relative step cycle phase) between the left front leg and each other leg was not  
 275 significantly different between CxHP8-silenced and control flies. A Kuiper two-sample test with a Bonferroni correction of 5 determined significance  
 276 (n.s.:  $p > 0.01$ ). N: number of flies; n: number of phase comparisons. See also Figure S4.

277

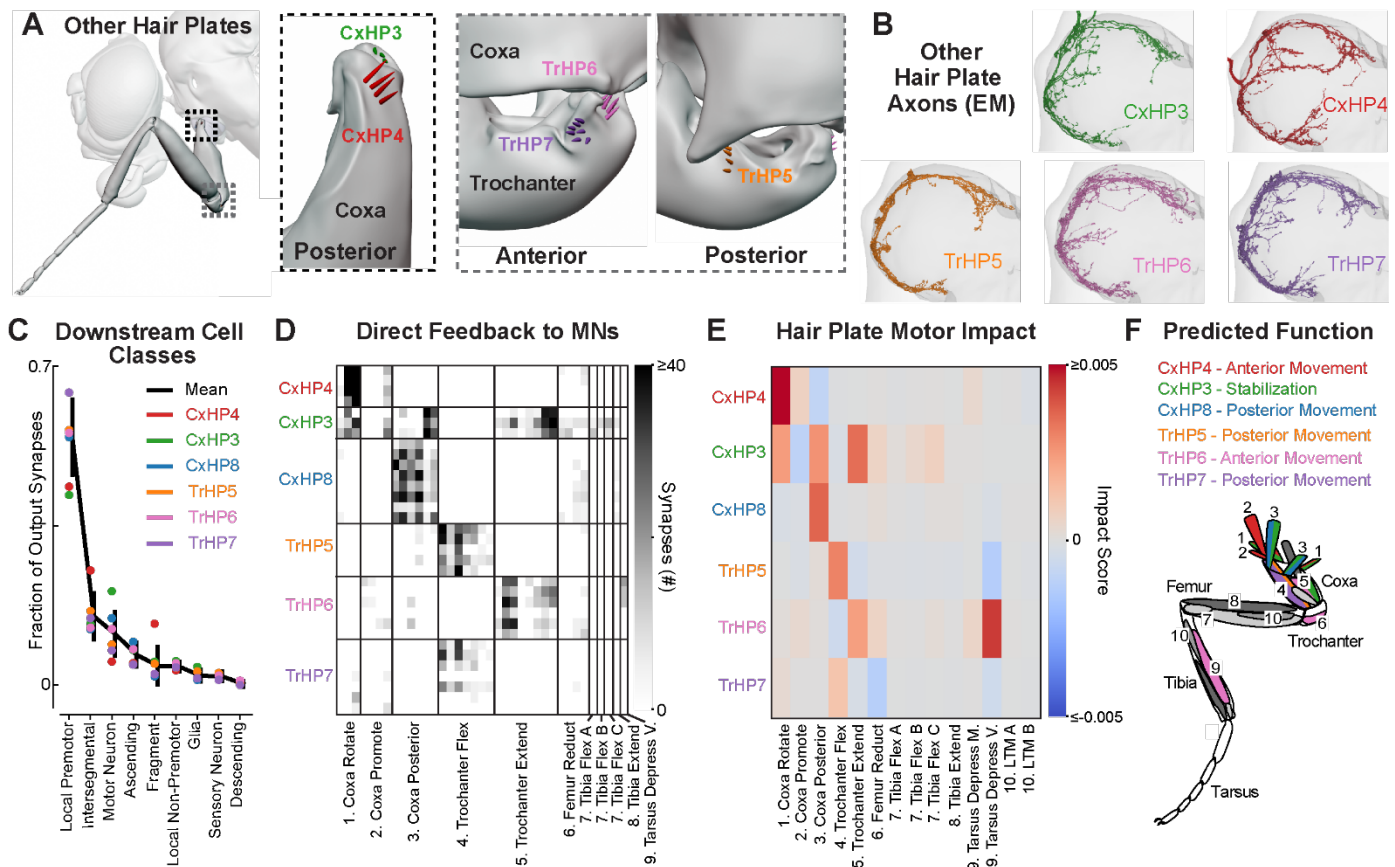
## 278 **Connectome analysis enables functional predictions for other hair plates on the fly leg**

279

280 Our calcium imaging data indicate that CxHP8 neurons function as limit detectors of anterior coxa movement (Figure 1).  
 281 Based on analysis of the connectome, we hypothesized that feedback from CxHP8 neurons helps transition the coxa away  
 282 from its anterior limit by driving posterior movement (Figure 2). We tested and confirmed this prediction by genetically  
 283 manipulating the activity of CxHP8 neurons in behaving flies (Figures 3,4). Having validated the predicted reflex function  
 284 for one hair plate, we now return to the connectome to predict the role of other front leg hair plates in leg motor control.

285 We focused on the two other hair plates on the front leg coxa, CxHP3 and CxHP4, along with the three hair plates located  
 286 at the coxa-trochanter joint, TrHP5, TrHP6, and TrHP7 (Figure 5A). In FANC, we reconstructed the axons of each of

287 these hair plates (**Figure 5B, S5A**). Of the thousands of output synapses from these hair plate axons (**Figure S5B**),  
 288 the majority of synapses are onto local premotor and motor neurons (**Figure 5C**). Interestingly, we also found that some hair  
 289 plate axons synapse onto glia, suggesting that their signaling may be used for non-motor related functions, such as  
 290 detecting injury (**Figures 5C, S5C**). The axons of each hair plate connect to distinct populations of motor neurons that  
 291 actuate the leg segment the hair plate is located on (**Figure 5D**). For instance, CxHP4 axons provide strong connectivity  
 292 to motor neurons of the coxa rotate motor module, which drives anterior coxa movement, whereas the antagonistically  
 293 positioned CxHP8, connects to the antagonistic coxa posterior motor module. We also found that the axons of each hair  
 294 plate synapse onto diverse premotor neurons (**Figure S5D**). By combining the connectivity of hair plates onto premotor  
 295 and motor neurons, we constructed 2-layer sensorimotor circuits for each hair plate (**Figure S5E**). We also computed the  
 296 motor impact score for each hair plate (**Figure 5E**), a measure that weights direct and indirect connectivity between  
 297 sensory and motor neurons, incorporating the neurotransmitter of any intervening interneurons (Lee et al., 2024). This  
 298 impact score is useful to understand trends or differences in motor connectivity, but, importantly, does not consider factors  
 299 such as activity dynamics or intrinsic neural properties. Nonetheless, comparing impact scores revealed clear differences  
 300 in motor connectivity among hair plates on different parts of the leg. For example, our analysis predicts that CxHP4 drives  
 301 anterior leg movement, CxHP3 reinforces both anterior and posterior leg movement, TrHP5 and TrHP7 drive posterior  
 302 leg movement, and TrHP6 drives anterior leg movement. Overall, the connectivity of hair plates suggests each limit  
 303 detector is specialized for controlling specific leg movements that are matched to the different extremes of joint movement  
 304 that they detect.



305

306 **Figure 5. Synaptic connectivity of hair plate axons indicates distinct roles in leg motor control.** (A) Hair plates located at the thorax-coxa (black  
 307 dotted box) and coxa-trochanter (gray dotted box) joints of the front leg. Schematics were rendered in Blender and based on high-resolution confocal  
 308 images. We focused on two hair-plates, in addition to CxHP8, located at the thorax-coxa joint (CxHP4: red; CxHP3: green) and three at the coxa-  
 309 trochanter joint (TrHP5: orange; TrHP7: purple; TrHP6: pink). (B) Reconstructed hair plate axons within the left front leg neuromere of FANC. (C)

310 Fraction of hair plate axon output synapses onto VNC cell classes. Black line: mean fraction of output synapses across all hair plate axons; Color  
311 dot: mean fraction of output synapses for the axons of each hair plate. (D) Connectivity matrix shows the number of synapses that motor neurons  
312 receive from hair plate axons. Axons from the same hair plate are grouped together (rows) while motor neurons within their defined motor module  
313 are arranged according to the proportion of input synapses they receive from specific hair plate axons. The leg muscles corresponding to the motor  
314 modules 1-9 are shown in F. (E) Motor impact scores (Lee et al., 2024), weighted sums of direct (monosynaptic) and indirect (di-synaptic) signed  
315 connection strengths, of hair plates onto leg motor modules. Red and blue hues correspond to excitatory and inhibitory impact scores, respectively.  
316 The leg muscles corresponding to the motor modules 1-10 are shown in F. See **Methods** for more information on how the motor impact score was  
317 calculated. (F) Predicted function and muscles controlled by each hair plate, as indicated by corresponding colors. See also **Figure S5** and **Video 2**.  
318

## 319 **Discussion**

320

321 In this study, we analyzed the physiology, circuit connectivity, and behavioral function of hair plates on the fly leg. We  
322 first used calcium imaging to discover that the neurons of one hair plate (CxHP8) are tonically active at the anterior  
323 extremes of coxa movement (**Figure 1**). We then used connectomics to predict that feedback from CxHP8 neurons drives  
324 posterior coxa and leg movement (**Figure 2**). Optogenetic stimulation of CxHP8 neurons was sufficient to drive reflexive  
325 posterior leg movements (**Figure 3**). We also found that optogenetic and chronic silencing of CxHP8 neurons in tethered  
326 flies (**Figure 3**) and flies walking freely on an actuated treadmill (**Figure 4**), caused the leg to overshoot the swing-to-  
327 stance transition in a medial direction. In addition to their role in walking, silencing CxHP8 neurons altered the resting  
328 position of the legs (**Figure S4**). Overall, these results agree with the sensorimotor reflex predictions from the connectome.  
329 We also provide functional predictions for the other hair plates on the front leg (**Figure 5**), which can be tested in future  
330 experiments as new genetic driver lines become available. Altogether, this work illustrates an integrated approach,  
331 anchored in the connectome, to infer the sensorimotor functions of spatially distributed proprioceptors.

332 Proprioceptive limit detectors are common in limbed animals. Nearly fifty years ago, recordings from joint receptors in  
333 the cat leg found that single afferents fired in a phasic or tonic manner as they neared the limit of the range of joint  
334 movement (Burgess and Clark, 1969). Previous electrophysiological work in locusts (BrÄunig and Hustert, 1985a, 1985b;  
335 Haskell, 1959; Kuenzi and Burrows, 1995; Newland et al., 1995) and cockroaches (French and Sanders, 1979; French and  
336 Wong, 1976; Pearson et al., 1976; Wong and Pearson, 1976) also found neurons within the same hair plate had either  
337 tonic or phasic encoding properties. However, we found no evidence for phasic tuning among CxHP8 axons – calcium  
338 signals remained sustained when the leg was held at an extreme position. It is possible that all hair plate neurons in the  
339 fly have tonic encoding properties. It is also possible that other hair plate neurons, which we did not record from in this  
340 study, respond phasically to mechanical stimulation. More work is needed to determine whether physiological properties  
341 vary across different hair plates.

342 While extensive prior work has investigated the encoding properties of proprioceptive limit detectors in other animals,  
343 less was known about their downstream connectivity and contributions to leg motor control during behavior. We found  
344 that activating and silencing CxHP8 neurons confirmed our leg motor control predictions based on connectivity. It is  
345 worth noting that the VNC circuits connecting hair plates and leg motor neurons are far more complex than our behavioral  
346 results and past work would suggest. For example, CxHP8 neurons also disynaptically excite and/or inhibit motor neurons  
347 controlling every other segment within the leg (**Figure 2B**), suggesting leg-wide rather than leg segment-specific motor  
348 control. Premotor neurons downstream of hair plates are also recurrently connected in complex patterns, and some synapse  
349 back onto CxHP8 axons (**Figure S2B**). This dense connectivity may support inter-joint coordination or provide robustness  
350 to external perturbations that the animal faces while navigating complex terrain.

351 Reflex circuits may also be modulated (i.e., suppressed or amplified) during different behavioral contexts. Hook (but not  
352 claw) proprioceptors in the fly femoral chordotonal organ (FeCO) are presynaptically inhibited during self-generated leg  
353 movements (Dallmann et al., 2023). Here, we did not observe suppression of hair plate calcium activity during  
354 spontaneous leg movements (**Figure 1**). Interestingly, optogenetic silencing of CxHP8 neurons had a significant, but

355 relatively small, effect on extreme anterior extension of the coxa during front leg grooming (**Figure S3D**), even though  
356 CxHP8 neurons showed strong activity during this behavior (**Figures 1J, S1D, Video 3**). Gain modulation could occur in  
357 downstream premotor neurons to fine-tune the reflex action of hair plates.

358 The fruit fly's front leg contains over 200 proprioceptive sensory neurons, including hair plates, campaniform sensilla,  
359 and chordotonal neurons (Kuan et al., 2020). Chordotonal neurons are primarily concentrated in the FeCO, which senses  
360 the femur/tibia joint (Mamiya et al., 2018). The more proximal coxa and trochanter joints contain similar numbers of  
361 campaniform sensilla and hair plates. Connectomic and electrophysiological evidence suggest that signals from these  
362 different proprioceptor classes are highly integrated in downstream circuits. For instance, work in the stick insect has  
363 shown that load and movement signals encoded by campaniform sensilla and FeCO neurons, respectively, are integrated  
364 in premotor networks to control the femur-tibia joint (Gebehart et al., 2021). Similarly, in the fly, electrophysiology and  
365 calcium imaging has revealed that signals from functional subtypes of FeCO neurons (i.e., claw, hook, club) are integrated  
366 in downstream neurons (Agrawal et al., 2020; Chen et al., 2021). Connectomic reconstruction has also revealed  
367 convergence of claw, hook, hair plate, and campaniform sensilla in downstream VNC neurons (Lee et al., 2024).  
368 Altogether, integration of signals across diverse proprioceptors may contribute to locomotor robustness and could also  
369 help explain why silencing CxHP8 neurons had only a very subtle effect on joint kinematics during walking.

370 Here, we focused on local reflex action of hair plates within a single leg. Hair plate axons do not project intersegmentally,  
371 and the majority of their disynaptic connectivity is also onto motor neurons controlling the same leg. However, past work  
372 has shown that hair plates may also contribute to intersegmental coordination across legs. In stick insects, for example,  
373 the ablation of hair plates on the middle leg resulted in non-linear and greater shifts in the anterior extreme position of the  
374 ipsilateral hind leg (Cruse et al., 1984). We did not observe kinematic changes of other legs when manipulating CxHP8  
375 neurons on the fly's left front leg. However, intersegmental effects could be driven by other hair plates.

376 Unlike other senses with a dedicated and localized organ like an eye, ear, or nose, proprioception is a distributed sense  
377 that relies on mechanosensory neurons distributed throughout the body. Therefore, a fundamental challenge for  
378 understanding proprioception is that the same class of sensory neurons in different locations may be anatomically  
379 specialized to detect specific perturbations to the body. Investigating hundreds or thousands of proprioceptors, one-by-  
380 one, is experimentally intractable. A promising future approach to overcome this problem is to combine the methods used  
381 above (connectomics, calcium imaging, and genetic manipulations during behavior) with biomechanical modeling  
382 (Vaxenburg et al., 2024; Wang-Chen et al., 2023). To facilitate this effort, we have added all of the hair plates  
383 characterized in this study to the open-source *Janelia* fly body Blender model (Vaxenburg et al., 2024) (**Video 2**). As other  
384 components are added to the body model, it will become possible to simulate hair plate signaling through recurrent,  
385 connectome-constrained networks. In the future, integrating biomechanical and connectome-constrained network models  
386 may provide a promising solution to the challenge of understanding how distributed sensory systems, including  
387 proprioception, control complex behaviors.

## 388 **Acknowledgements**

389 We thank members of the Tuthill and Brunton Labs for technical assistance and feedback on the manuscript. We thank  
390 Seok Jun Moon for sharing the CxHP8 split-GAL4 driver line (R48A07 AD: R20C06 DBD). B.G.P was supported by an  
391 NSF Graduate Research Fellowship (Fellow ID: 2018261272). C.J.D was supported from the Deutsche  
392 Forschungsgemeinschaft (DFG, German Research Foundation) project 432196121. Other support was provided by  
393 National Institutes of Health grants R01NS102333, R01NS128785, and U19NS104655, a Searle Scholar Award, a  
394 Klingenstein-Simons Fellowship, a Pew Biomedical Scholar Award, a McKnight Scholar Award, a Sloan Research  
395 Fellowship, the New York Stem Cell Foundation, and a UW Innovation Award to J.C.T. J.C.T is a New York Stem Cell  
396 Foundation – Robertson Investigator.

397

## 398 **Author Contributions**

399 B.G.P. and J.C.T. conceived the study and wrote the manuscript. I.S. created the gorgeous Blender model of a fruit fly  
400 with hair plates, as well as Video 2. B.G.P and A.S. performed confocal imaging of hair plates. B.G.P. and A.C. proofread  
401 the hair plate axons and their downstream and upstream partners in FANC. C.J.D. collected and processed the calcium  
402 imaging data for CxHP8. G.M.C. and S.W.B. collected optogenetic activation and silencing datasets for CxHP8. B.G.P.  
403 analyzed the connectivity, calcium imaging, and optogenetic datasets. B.G.P collected and analyzed the kinematics and  
404 posture of flies walking in the treadmill setup. A.A. provided valuable feedback about the connectivity of hair plates onto  
405 motor circuits.

## 407 **Declaration of Interests**

408 J.C.T. is a member of Current Biology's advisory board.

## 410 **Lead contact**

411 Further information and requests for resources and reagents should be directed to and will be fulfilled by the lead contact,  
412 John C. Tuthill ([tuthill@uw.edu](mailto:tuthill@uw.edu)).

## 414 **Data and Code Availability**

415 Data is available on Dryad (DOI: 10.5061/dryad.fxpnvx153). Code for analyzing and visualizing hair plate connectivity  
416 in the EM dataset, calcium activity of CxHP8 neurons, kinematics during optogenetic experiments, and walking  
417 kinematics and posture during treadmill experiments is located on GitHub  
418 ([https://github.com/Prattbuw/Hair\\_Plate\\_Paper](https://github.com/Prattbuw/Hair_Plate_Paper)).

## 420 **References**

- 421 Agrawal S, Dickinson ES, Sustar A, Gurung P, Shepherd D, Truman JW, Tuthill JC. 2020. Central processing of leg  
422 proprioception in *Drosophila*. *Elife* **9**:e60299. doi:10.7554/eLife.60299
- 423 Akitake B, Ren Q, Boiko N, Ni J, Sokabe T, Stockand JD, Eaton BA, Montell C. 2015. Coordination and fine motor  
424 control depend on *Drosophila* TRP $\gamma$ . *Nat Commun* **6**. doi:10.1038/ncomms8288
- 425 Azevedo A, Lesser E, Phelps JS, Mark B, Elabbady L, Kuroda S, Sustar A, Moussa A, Khandelwal A, Dallmann CJ,  
426 Agrawal S, Lee S-YJ, Pratt B, Cook A, Skutt-Kakaria K, Gerhard S, Lu R, Kemnitz N, Lee K, Halageri A,  
427 Castro M, Ih D, Gager J, Tammam M, Dorckenwald S, Collman F, Schneider-Mizell C, Brittain D, Jordan  
428 CS, Dickinson M, Pacureanu A, Seung HS, Macrina T, Lee W-CA, Tuthill JC. 2024. Connectomic  
429 reconstruction of a female *Drosophila* ventral nerve cord. *Nature* **631**:360–368. doi:10.1038/s41586-024-  
430 07389-x
- 431 Azevedo AW, Dickinson ES, Gurung P, Venkatasubramanian L, Mann RS, Tuthill JC. 2020. A size principle for  
432 recruitment of *Drosophila* leg motor neurons. *eLife* **9**:e56754. doi:10.7554/eLife.56754
- 433 Bässler U. 1977. Sensory control of leg movement in the stick insect *Carausius morosus*. *Biological Cybernetics*  
434 **25**:61–72. doi:10.1007/BF00337264
- 435 BrÄunig P, Hustert R. 1985a. Actions and interactions of proprioceptors of the locust hind leg coxo-trochanteral  
436 joint. *Journal of Comparative Physiology A* **157**:83–89. doi:10.1007/BF00611098
- 437 BrÄunig P, Hustert R. 1985b. Actions and interactions of proprioceptors of the locust hind leg coxo-trochanteral  
438 joint. *Journal of Comparative Physiology A* **157**:73–82. doi:10.1007/BF00611097
- 439 Burgess PR, Clark FJ. 1969. Characteristics of knee joint receptors in the cat. *The Journal of Physiology* **203**:317–  
440 335. doi:10.1113/jphysiol.1969.sp008866
- 441 Chen C, Agrawal S, Mark B, Mamiya A, Sustar A, Phelps JS, Lee W-CA, Dickson BJ, Card GM, Tuthill JC. 2021.  
442 Functional architecture of neural circuits for leg proprioception in *Drosophila*. *Current Biology* **31**:5163–  
443 5175. doi:10.1016/j.cub.2021.09.035
- 444 Cheng LE, Song W, Looger LL, Jan LY, Jan YN. 2010. The Role of the TRP Channel NompC in *Drosophila* Larval  
445 and Adult Locomotion. *Neuron* **67**:373–380. doi:10.1016/j.neuron.2010.07.004

446 Chockley AS, Dinges GF, Di Cristina G, Ratican S, Bockemühl T, Büschges A. 2022. Subsets of leg proprioceptors  
447 influence leg kinematics but not interleg coordination in *Drosophila melanogaster* walking. *Journal of*  
448 *Experimental Biology* **225**:jeb244245. doi:10.1242/jeb.244245

449 Clark FJ, Horch KW, Bach SM, Larson GF. 1979. Contributions of cutaneous and joint receptors to static knee-  
450 position sense in man. *Journal of Neurophysiology* **42**:877–888. doi:10.1152/jn.1979.42.3.877

451 Cruse H, Dean J, Suilmann M. 1984. The contributions of diverse sense organs to the control of leg movement by a  
452 walking insect. *Journal of Comparative Physiology A* **154**:695–705. doi:10.1007/BF01350223

453 Dallmann CJ, Agrawal S, Cook A, Brunton BW, Tuthill JC. 2023. Presynaptic inhibition selectively suppresses leg  
454 proprioception in behaving *Drosophila*. *bioRxiv* 2023.10.20.563322.  
455 doi:10.1101/2023.10.20.563322

456 DeAngelis BD, Zavatone-Veth JA, Clark DA. 2019. The manifold structure of limb coordination in walking  
457 *Drosophila*. *eLife* **8**:e46409. doi:10.7554/eLife.46409

458 Dorkenwald S, Matsliah A, Sterling AR, Schlegel P, Yu S-C, McKellar CE, Lin A, Costa M, Eichler K, Yin Y,  
459 Silversmith W, Schneider-Mizell C, Jordan CS, Brittain D, Halageri A, Kuehner K, Ogedengbe O, Morey R,  
460 Gager J, Kruk K, Perlman E, Yang R, Deutsch D, Bland D, Sorek M, Lu R, Macrina T, Lee K, Bae JA, Mu  
461 S, Nehoran B, Mitchell E, Popovych S, Wu J, Jia Z, Castro MA, Kemnitz N, Ih D, Bates AS, Eckstein N,  
462 Funke J, Collman F, Bock DD, Jefferis GSXE, Seung HS, Murthy M, FlyWire Consortium. 2024. Neuronal  
463 wiring diagram of an adult brain. *Nature* **634**:124–138. doi:10.1038/s41586-024-07558-y

464 French AS, Sanders EJ. 1979. The mechanism of sensory transduction in the sensilla of the trochanteral hair plate of  
465 the cockroach, *Periplaneta americana*. *Cell and Tissue Research* **198**:159–174. doi:10.1007/BF00234843

466 French AS, Wong RKS. 1976. The responses of trochanteral hair plate sensilla in the cockroach to periodic and  
467 random displacements. *Biological Cybernetics* **22**:33–38. doi:10.1007/BF00340230

468 Gebehart C, Schmidt J, Büschges A. 2021. Distributed processing of load and movement feedback in the premotor  
469 network controlling an insect leg joint. *Journal of Neurophysiology* **125**:1800–1813.  
470 doi:10.1152/jn.00090.2021

471 Grigg P, Finerman GA, Riley LH. 1973. Joint-Position Sense after Total Hip Replacement. *JBJS* **55**.

472 Guizar-Sicairos M, Thurman ST, Fienup JR. 2008. Efficient subpixel image registration algorithms. *Optics letters*  
473 **33**:156–158. doi:10.1364/OL.33.000156

474 Harris RM, Pfeiffer BD, Rubin GM, Truman JW. 2015. Neuron hemilineages provide the functional ground plan for  
475 the *Drosophila* ventral nervous system. *eLife* **4**:e04493. doi:10.7554/eLife.04493

476 Haskell PT. 1959. Hair Receptors in Locusts: Function of certain Prothoracic Hair Receptors in the Desert Locust.  
477 *Nature* **183**:1107–1107.

478 Hodgkin HM, Bryant PJ. 1979. Scanning electron microscopy of the adult of *Drosophila melanogaster*. *Genetics and*  
479 *biology of Drosophila* **2**.

480 Isakov A, Buchanan SM, Sullivan B, Ramachandran A, Chapman JKS, Lu ES, Mahadevan L, de Bivort B. 2016.  
481 Recovery of locomotion after injury in *Drosophila melanogaster* depends on proprioception. *Journal of*  
482 *Experimental Biology* **219**:1760–1771. doi:10.1242/jeb.133652

483 Jenett A, Rubin GM, Ngo T-TB, Shepherd D, Murphy C, Dionne H, Pfeiffer BD, Cavallaro A, Hall D, Jeter J, Iyer  
484 N, Fetter D, Hausenfluck JH, Peng H, Trautman ET, Svirskas RR, Myers EW, Iwinski ZR, Aso Y,  
485 DePasquale GM, Enos A, Hulamm P, Lam SCB, Li H-H, Lavery TR, Long F, Qu L, Murphy SD, Rokicki  
486 K, Safford T, Shaw K, Simpson JH, Sowell A, Tae S, Yu Y, Zugates CT. 2012. A GAL4-driver line resource  
487 for *Drosophila* neurobiology. *Cell Rep* **2**:991–1001. doi:10.1016/j.celrep.2012.09.011

488 Karashchuk P, Rupp KL, Dickinson ES, Walling-Bell S, Sanders E, Azim E, Brunton BW, Tuthill JC. 2021.  
489 Anipose: A toolkit for robust markerless 3D pose estimation. *Cell Rep* **36**:109730.  
490 doi:10.1016/j.celrep.2021.109730

491 Kuan AT, Phelps JS, Thomas LA, Nguyen TM, Han J, Chen C-L, Azevedo AW, Tuthill JC, Funke J, Cloetens P,  
492 Pacureanu A, Lee W-CA. 2020. Dense neuronal reconstruction through X-ray holographic nano-  
493 tomography. *Nature Neuroscience* **1–7**. doi:10.1038/s41593-020-0704-9

494 Kuenzi F, Burrows M. 1995. Central Connections of Sensory Neurones From a Hair Plate Proprioceptor in the  
495 Thoraco-Coxal Joint of the Locust. *Journal of Experimental Biology* **198**:1589–1601.  
496 doi:10.1242/jeb.198.7.1589

497 Lacin H, Chen H-M, Long X, Singer RH, Lee T, Truman JW. 2019. Neurotransmitter identity is acquired in a  
498 lineage-restricted manner in the *Drosophila* CNS. *Elife* **8**. doi:10.7554/eLife.43701

499 Lee S-YJ, Dallmann CJ, Cook A, Tuthill JC, Agrawal S. 2024. Divergent neural circuits for proprioceptive and  
500 exteroceptive sensing of the *Drosophila* leg. *bioRxiv* 2024.04.23.590808.  
501 doi:10.1101/2024.04.23.590808

502 Lesser E, Azevedo AW, Phelps JS, Elabbady L, Cook A, Syed DS, Mark B, Kuroda S, Sustar A, Moussa A,  
503 Dallmann CJ, Agrawal S, Lee S-YJ, Pratt B, Skutt-Kakaria K, Gerhard S, Lu R, Kemnitz N, Lee K, Halageri  
504 A, Castro M, Ih D, Gager J, Tammam M, Dorkenwald S, Collman F, Schneider-Mizell C, Brittain D, Jordan  
505 CS, Macrina T, Dickinson M, Lee W-CA, Tuthill JC. 2024. Synaptic architecture of leg and wing premotor  
506 control networks in *Drosophila*. *Nature* **631**:369–377. doi:10.1038/s41586-024-07600-z

507 Maitin-Shepard J, Baden A, Silversmith W, Perlman E, Collman F, Blakely T, Funke J, Jordan C, Falk B, Kemnitz  
508 N, tingzhao, Roat C, Castro M, Jagannathan S, moenigin, Clements J, Hoag A, Katz B, Parsons D, Wu J,  
509 Kamentsky L, Chervakov P, Hubbard P, Berg S, Hoffer J, Halageri A, Machacek C, Mader K, Roeder L, Li  
510 PH. 2021. google/neuroglancer: doi:10.5281/zenodo.5573294

511 Mamiya A, Gurung P, Tuthill JC. 2018. Neural Coding of Leg Proprioception in *Drosophila*. *Neuron* **100**:636-  
512 650.e6. doi:10.1016/j.neuron.2018.09.009

513 Mamiya A, Sustar A, Siwanowicz I, Qi Y, Lu T-C, Gurung P, Chen C, Phelps JS, Kuan AT, Pacureanu A, Lee W-  
514 CA, Li H, Mhatre N, Tuthill JC. 2023. Biomechanical origins of proprioceptor feature selectivity and  
515 topographic maps in the *Drosophila* leg. *Neuron* **111**:3230-3243.e14. doi:10.1016/j.neuron.2023.07.009

516 Marin EC, Morris BJ, Stürner T, Champion AS, Krzeminski D, Badalamente G, Gkantia M, Dunne CR, Eichler K,  
517 Takemura S, Tamimi IF, Fang S, Moon SS, Cheong HS, Li F, Schlegel P, Ahnert SE, Berg S, Team JFP,  
518 Card GM, Costa M, Shepherd D, Jefferis GS. 2024. Systematic annotation of a complete adult male  
519 *Drosophila* nerve cord connectome reveals principles of functional organisation. *eLife* **13**.  
520 doi:10.7554/eLife.97766.1

521 Mathis A, Mamidanna P, Cury KM, Abe T, Murthy VN, Mathis MW, Bethge M. 2018. DeepLabCut: markerless  
522 pose estimation of user-defined body parts with deep learning. *Nature Neuroscience* **21**:1281.  
523 doi:10.1038/s41593-018-0209-y

524 Mendes CS, Bartos I, Akay T, Márka S, Mann RS. 2013. Quantification of gait parameters in freely walking wild  
525 type and sensory deprived *Drosophila melanogaster*. *eLife Sciences* **2**:e00231. doi:10.7554/eLife.00231

526 Moore RJD, Taylor GJ, Paulk AC, Pearson T, van Swinderen B, Srinivasan MV. 2014. FicTrac: A visual method for  
527 tracking spherical motion and generating fictive animal paths. *Journal of Neuroscience Methods* **225**:106–  
528 119. doi:10.1016/j.jneumeth.2014.01.010

529 Newland PL, Watkins B, Emptage NJ, Nagayama T. 1995. The Structure, Response Properties and Development of a  
530 Hair Plate on the Mesothoracic Leg of the Locust. *Journal of Experimental Biology* **198**:2397–2404.  
531 doi:10.1242/jeb.198.11.2397

532 Oh SM, Jeong K, Seo JT, Moon SJ. 2021. Multisensory interactions regulate feeding behavior in *Drosophila*.  
533 *Proceedings of the National Academy of Sciences* **118**:e2004523118. doi:10.1073/pnas.2004523118

534 Pearson KG, Wong RK, Fournier CR. 1976. Connexions between hair-plate afferents and motoneurons in the  
535 cockroach leg. *Journal of Experimental Biology* **64**:251–266. doi:10.1242/jeb.64.1.251

536 Phelps JS, Hildebrand DGC, Graham BJ, Kuan AT, Thomas LA, Nguyen TM, Buhmann J, Azevedo AW, Sustar A,  
537 Agrawal S, Liu M, Shanny BL, Funke J, Tuthill JC, Lee W-CA. 2021. Reconstruction of motor control  
538 circuits in adult *Drosophila* using automated transmission electron microscopy. *Cell* **184**:759-774.e18.  
539 doi:10.1016/j.cell.2020.12.013

540 Pratt BG, Lee S-YJ, Chou GM, Tuthill JC. 2024. Miniature linear and split-belt treadmills reveal mechanisms of  
541 adaptive motor control in walking *Drosophila*. *Curr Biol* **34**:4368-4381.e5. doi:10.1016/j.cub.2024.08.006

542 Pringle JWS. 1938. Proprioception in Insects: III. The Function of the Hair Sensilla at the Joints. *Journal of*  
543 *Experimental Biology* **15**:467–473. doi:10.1242/jeb.15.4.467

544 Proske U, Gandevia SC. 2012. The Proprioceptive Senses: Their Roles in Signaling Body Shape, Body Position and  
545 Movement, and Muscle Force. *Physiological Reviews* **92**:1651–1697. doi:10.1152/physrev.00048.2011

546 Schindelin J, Arganda-Carreras I, Frise E, Kaynig V, Longair M, Pietzsch T, Preibisch S, Rueden C, Saalfeld S,  
547 Schmid B, Tinevez J-Y, White DJ, Hartenstein V, Eliceiri K, Tomancak P, Cardona A. 2012. Fiji: an open-  
548 source platform for biological-image analysis. *Nat Methods* **9**:676–682. doi:10.1038/nmeth.2019

549 Schubiger G. 1968. Anlageplan, Determinationszustand und Transdeterminationsleistungen der männlichen  
550 Vorderbeinscheibe von *Drosophila melanogaster*. *Wilhelm Roux' Archiv für Entwicklungsmechanik der*  
551 *Organismen* **160**:9–40. doi:10.1007/BF00573645

552 Strauss R, Heisenberg M. 1990. Coordination of legs during straight walking and turning in *Drosophila*  
553 *melanogaster*. *J Comp Physiol A* **167**:403–412.

554 Takemura Shin-ya, Hayworth KJ, Huang GB, Januszewski M, Lu Z, Marin EC, Preibisch S, Xu CS, Bogovic J,  
555 Champion AS, Cheong HS, Costa M, Eichler K, Katz W, Knecht C, Li F, Morris BJ, Ordish C, Rivlin PK,  
556 Schlegel P, Shinomiya K, Stürner T, Zhao T, Badalamente G, Bailey D, Brooks P, Canino BS, Clements J,  
557 Cook M, Duclos O, Dunne CR, Fairbanks K, Fang S, Finley-May S, Francis A, George R, Gkantia M,  
558 Harrington K, Hopkins GP, Hsu J, Hubbard PM, Javier A, Kainmueller D, Korff W, Kovalyak J, Krzemiński  
559 D, Lauchie SA, Lohff A, Maldonado C, Manley EA, Mooney C, Neace E, Nichols M, Ogundeyi O, Okeoma  
560 N, Paterson T, Phillips E, Phillips EM, Ribeiro C, Ryan SM, Rymer JT, Scott AK, Scott AL, Shepherd D,  
561 Shinomiya A, Smith C, Smith N, Suleiman A, Takemura Satoko, Talebi I, Tamimi IF, Trautman ET,  
562 Umayam L, Walsh JJ, Yang T, Rubin GM, Scheffer LK, Funke J, Saalfeld S, Hess HF, Plaza SM, Card GM,  
563 Jefferis GS, Berg S. 2024. A Connectome of the Male *Drosophila* Ventral Nerve Cord. *eLife* **13**.  
564 doi:10.7554/eLife.97769.1

565 Theunissen LM, Vikram S, Dürr V. 2014. Spatial co-ordination of foot contacts in unrestrained climbing insects.  
566 *Journal of Experimental Biology* **217**:3242–3253. doi:10.1242/jeb.108167

567 Tuthill JC, Azim E. 2018. Proprioception. *Curr Biol* **28**:R194–R203. doi:10.1016/j.cub.2018.01.064

568 Vaxenburg R, Siwanowicz I, Merel J, Robie AA, Morrow C, Novati G, Stefanidi Z, Card GM, Reiser MB, Botvinick  
569 MM, Branson KM, Tassa Y, Turaga SC. 2024. Whole-body simulation of realistic fruit fly locomotion with  
570 deep reinforcement learning. *bioRxiv* 2024.03.11.584515. doi:10.1101/2024.03.11.584515

571 Wang-Chen S, Stimpfling VA, Özdil PG, Genoud L, Hurtak F, Ramdya P. 2023. NeuroMechFly 2.0, a framework  
572 for simulating embodied sensorimotor control in adult *Drosophila*. *bioRxiv* 2023.09.18.556649.  
573 doi:10.1101/2023.09.18.556649

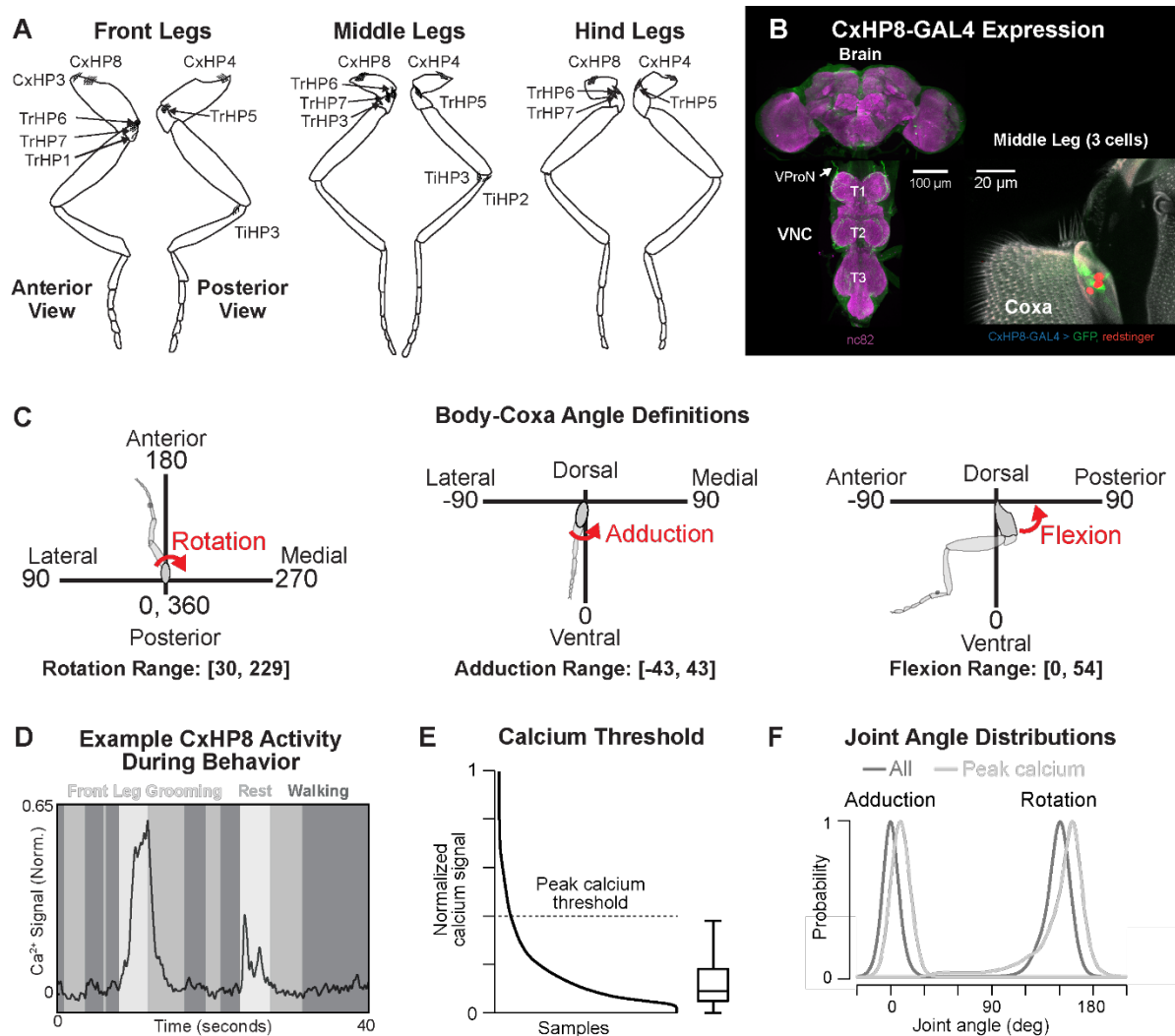
574 Wendler, G. 1972. Körperhaltung bei der Stabheuschrecke: Ihre Beziehung zur Schwereorientierung und  
575 Mechanismen ihrer Regelung. *Verhandlungen der Deutschen Zoologischen Gesellschaft* 214–219.

576 Winding M, Pedigo BD, Barnes CL, Patsolic HG, Park Y, Kazimiers T, Fushiki A, Andrade IV, Khandelwal A,  
577 Valdes-Aleman J, Li F, Randel N, Barsotti E, Correia A, Fetter RD, Hartenstein V, Priebe CE, Vogelstein  
578 JT, Cardona A, Zlatic M. 2022. The connectome of an insect brain. doi:10.1101/2022.11.28.516756

579 Wong RK, Pearson KG. 1976. Properties of the trochanteral hair plate and its function in the control of walking in  
580 the cockroach. *Journal of Experimental Biology* **64**:233–249. doi:10.1242/jeb.64.1.233

581 Wosnitza A, Bockemühl T, Dübber M, Scholz H, Büschges A. 2013. Inter-leg coordination in the control of walking  
582 speed in *Drosophila*. *Journal of Experimental Biology* **216**:480–491. doi:10.1242/jeb.078139

583  
584  
585  
586

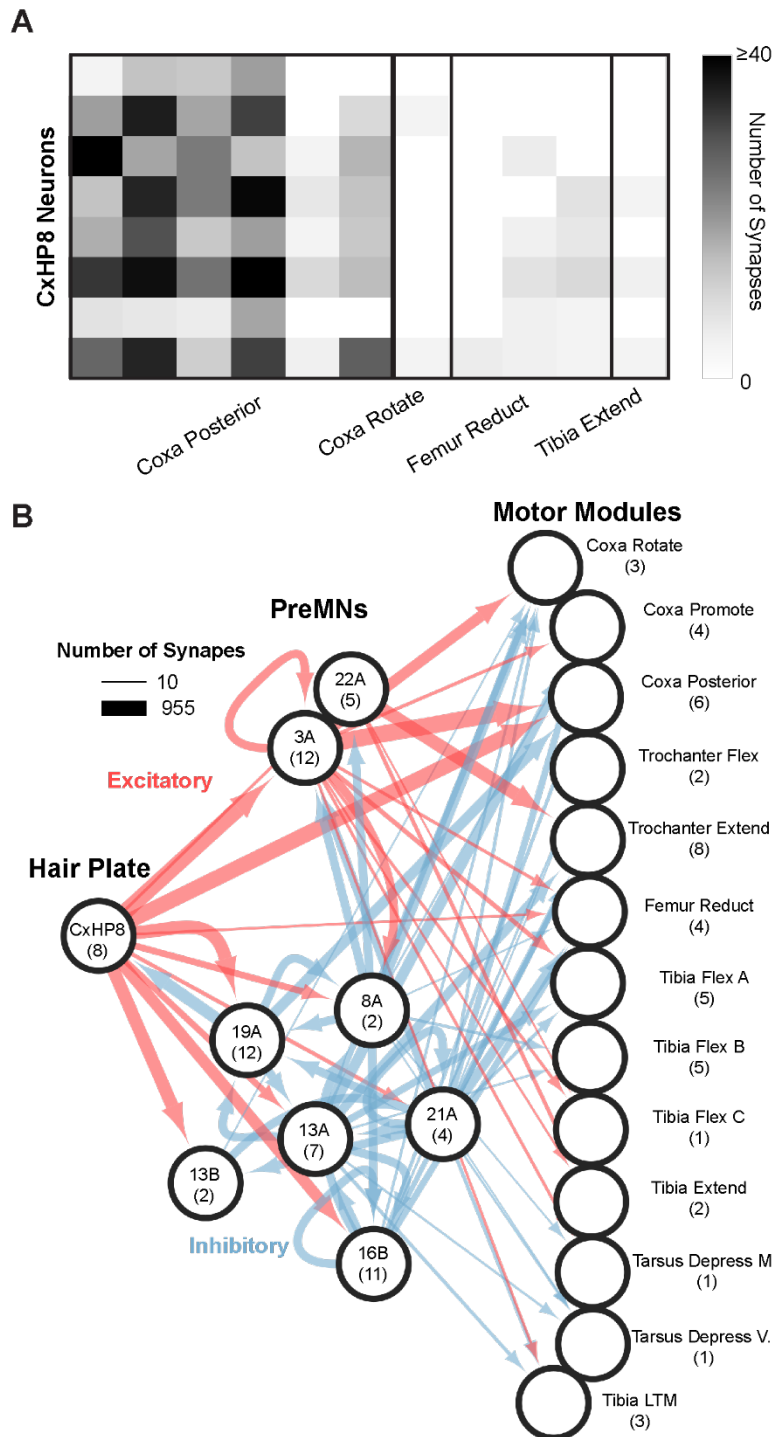


589

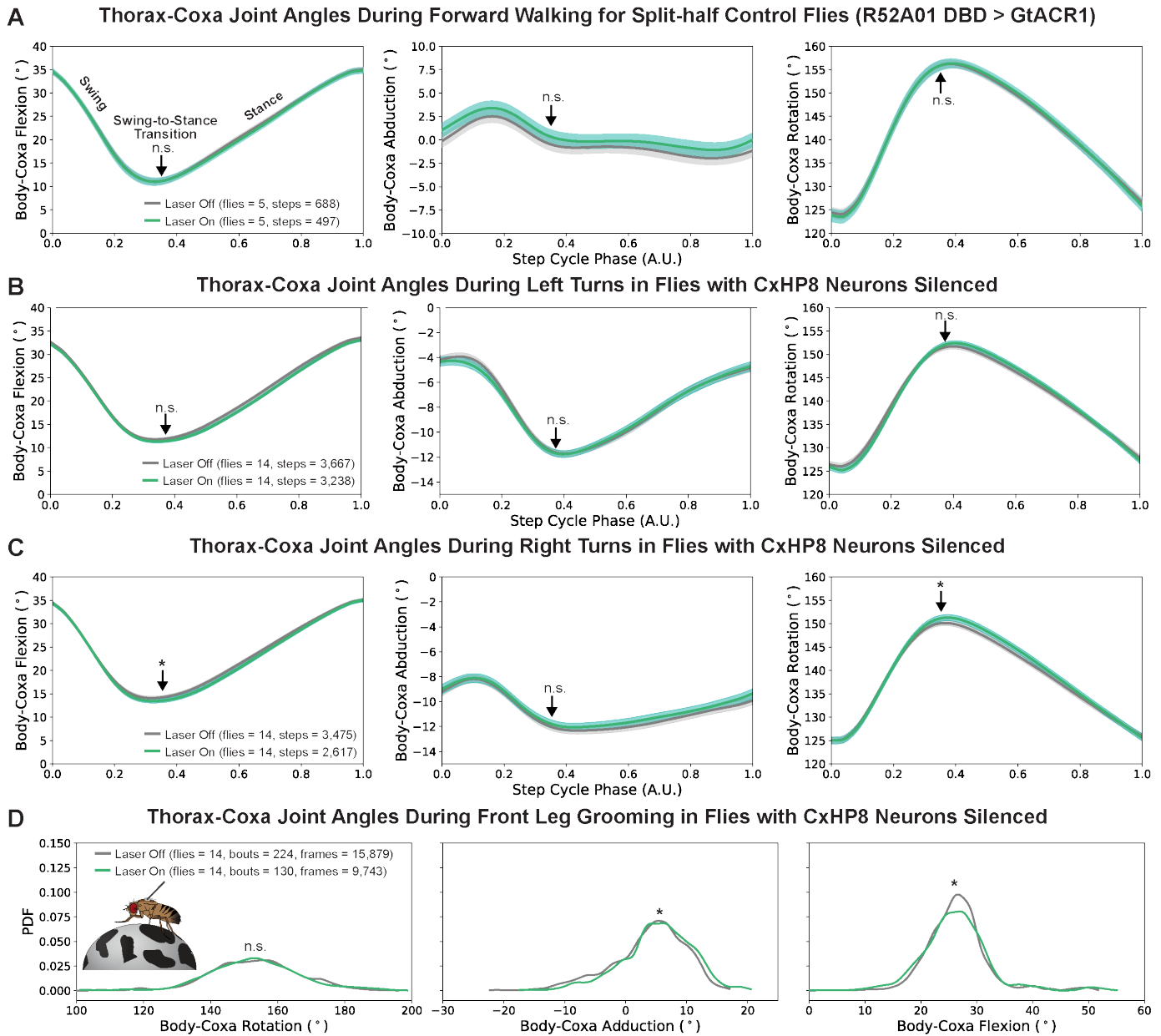
590 **Figure S1. Hair plate locations on the legs of *Drosophila*, CxHP8 driver line expression, and thorax-coxa joint angle definitions and encoding.**

591 (A) Schematics of the front, middle, and hind legs showing the locations of hair plates. (B) Confocal images showing the expression of the CxHP8  
 592 split-GAL4 in the middle leg (3 of 8 neurons labeled), brain, and VNC. The ultrastructure (autofluorescence: gray) of CxHP8 consists of 8 cuticular  
 593 hairs located on the coxa. Labeled mechanosensory neuron (GFP: green) project through the ventral prothoracic nerve (VProN) into the VNC (nc82:  
 594 magenta). The cell bodies of CxHP8 neurons are labeled by the nuclear marker, redstinger (red). (C) Reference frame for the rotation, adduction,  
 595 and flexion thorax-coxa angles of the front leg. The measured range of each angle is displayed at the bottom. (D) Example trial showing the  
 596 normalized calcium activity (normalized to the max calcium activity in the dataset) during front leg grooming, rest, and walking. (E) Calcium  
 597 threshold was set at the upper whisker limit ( $Q3 + 1.5 * IQR$ ) of the calcium activity box plot and was used for determining large peak calcium  
 598 activity events. (F) Adduction and rotation joint angle probability distributions during all calcium activity (gray) and just peak calcium events (light  
 599 gray).

600



601  
 602 **Figure S2. CxHP8 reflex circuit connectivity.** (A) CxHP8 connectivity onto motor neurons reveals that all CxHP8 axons primarily synapse onto  
 603 motor neurons within the coxa posterior motor module. The x-axis represents individual motor neurons within defined motor modules. (B) CxHP8  
 604 reflex circuit shown in **Figure 2B**, with the addition of premotor-to-premotor, and premotor-to-CxHP8 recurrent connections. Red and blue lines  
 605 indicate excitatory and inhibitory connections, respectively. The width of the line corresponds to the number of synapses between cell classes. The  
 606 number of neurons within each class are indicated within the parentheses. Note that only connections with greater than 3 synapses on average between  
 607 upstream neurons within a class and downstream cell classes were used in this analysis.  
 608

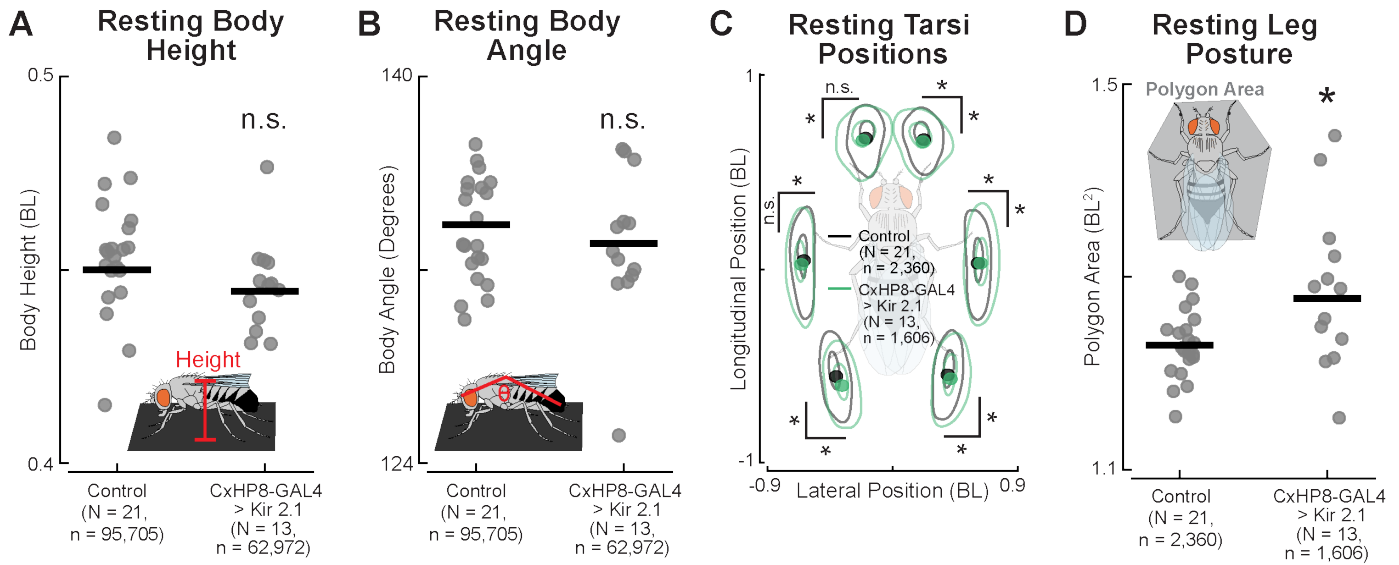


609

610

**Figure S3. Control flies had no significant change in joint angles during laser stimulation and CxHP8 silencing had significant effects on thorax-coxa joint angles during right turns and front leg grooming but not left turns.** (A) Control flies (R52A01 DBD > GtACR1) had no significant (n.s.:  $p > 0.025$ ) changes in coxa joint angles when the green laser was on compared to when it was off. Arrow: the average swing-to-stance transition of the step cycle; Shaded region: 95% confidence interval; N: number of flies; n: number of steps. A t-test with a Bonferroni correction of 2 was used to statistically compare the distributions of joint angles at the swing-to-stance transition. (B) Optogenetic silencing (green) of CxHP8 neurons in flies turning left didn't have a significant effect (t-test with a Bonferroni correction of 2; n.s.:  $p > 0.025$ ) on thorax-coxa angles compared to turning steps when the laser was off. (C) Optogenetic silencing of CxHP8 neurons had a significant (t-test; \*:  $p < 0.025$ ) effect on flexion and rotation angles at the swing-to-stance transition during right turns. (D) Optogenetic silencing (green) of CxHP8 neurons significantly (t-test with a Bonferroni correction of 2; \*:  $p < 0.025$ ) altered the thorax-coxa adduction and flexion joint angle during front leg grooming compared to when the laser was off (gray).

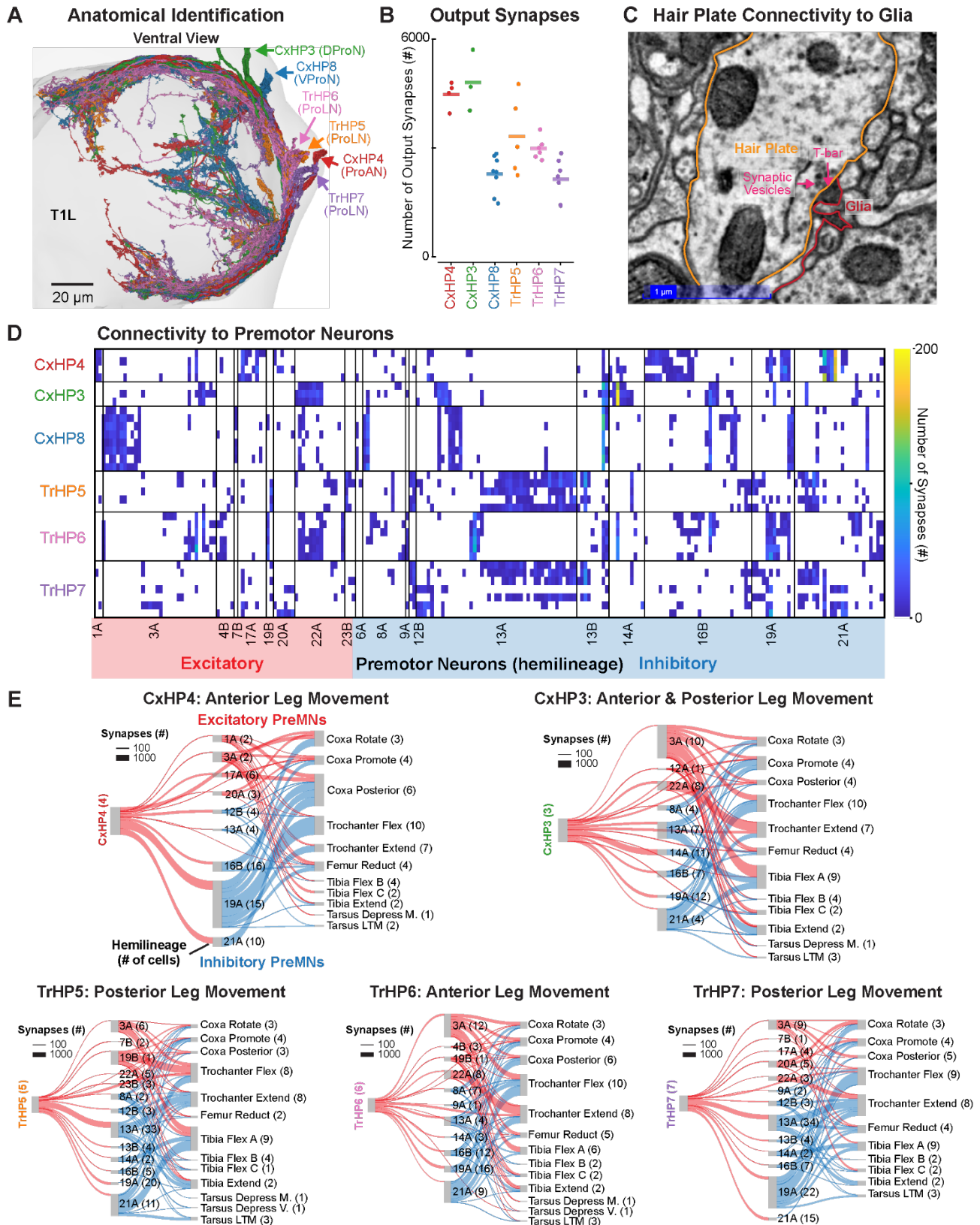
620



622

623

624 **Figure S4. CxHP8 feedback controls resting leg positions but not body height or angle.** (A) Body height was lower on average but not  
 625 significantly different between CxHP8 silenced and control flies (t-test;  $p > 0.05$ ). N: number of flies; n: number of frames. (B) Body angle was also  
 626 smaller on average but not significantly different between CxHP8 silenced and control flies (t-test;  $p > 0.05$ ). N: number of flies; n: number of frames.  
 627 (C) Resting positions of the tarsi during periods of standing were significantly different between CxHP8 silenced (green) and control (black) flies.  
 628 Distributions were determined by kernel density estimation. Dot: mean position; N: number of flies; n: number of resting bouts. Bootstrapping with  
 629 a Bonferroni correction was used to test for statistical differences (\*:  $p < 0.001$ ). (D) As quantified by polygon area, the resting posture of the legs  
 630 was significantly more spread out for flies with CxHP8 neurons silenced compared to controls (t-test; \*:  $p < 0.05$ ). N: number of flies; n: number of  
 631 resting bouts.



632

633

634

635

636

637

**Figure S5. Synaptic connectivity of hair plates in motor circuits and onto glia.** (A) Front leg hair plate axons are identified, in part, based on the nerve they project through and axonal morphology. DProN: dorsal prothoracic nerve; VProN: ventral prothoracic nerve; ProAN: prothoracic accessory nerve; ProLN: prothoracic leg nerve. (B) Total number of predicted output synapses of hair plate axons in FANC. Line: mean output synapses; dot: number of output synapses of a single hair plate axon. (C) Electron microscopy image illustrating the connectivity between a hair plate axon (orange) and a glia cell (red). Synaptic vesicles and a putative T-bar are labeled. (D) Connectivity matrix showing the number of synapses

638 that hair plate axons supply to premotor neurons. Premotor neurons are classified as excitatory (red) or inhibitory (blue) based on their identified  
639 hemilineage. Premotor neurons within a hemilineage are arranged according to the proportion of input synapses they receive from each hair plate  
640 axon. (E) Based on their connectivity with premotor and motor neurons, the neurons of each hair plate are predicted to engage reflex circuits that  
641 control distinct aspects of leg movement. Above each reflex circuit is the prediction for the associated hair plate in controlling leg movement. Only  
642 connections of at least 4 synapses on average per neuron within a cell class onto downstream cell classes were used to construct each reflex circuit.  
643 The number of cells in each cell class is indicated within the parentheses.

644  
645  
646

Driver Line	Front Leg Proprioceptors									Middle Leg Proprioceptors						Hind Leg Proprioceptors								
	CxHP4	CxHP3	CxHP8	TtHP5	TtHP6	TtHP7	TtHP1	TtCS3 (TrG)	TtCS5 (TrF <sub>0</sub> )	FeCS11	CxHP4	CxHP8	TtHP5	TtHP6	TtHP7	TtCS3	TtCS2	CxHP4	CxHP8	TtHP5	TtHP6	TtHP7	TtCS3	
R48A07 AD: R20C06 DBD	0	0	6	0	0	0	0	0	0	0	0	3	0	0	0	0	0	0	0	0	0	0	0	0
R93D09 AD: VT061711 DBD	2	0	4	3	0	0	0	3	0	0	0	6	3	3	1	2	0	4	6	3	4	2	0	0
R93D09 AD: VT009832 DBD	2	2	0	3	2	2	0	0	0	0	2	0	3	2	0	0	1	3	0	3	3	0	0	0
R93D09 AD: VT040055 DBD	1	0	0	2	0	0	0	2	0	0	2	0	0	0	0	2	0	2	0	0	0	0	0	2
R93D09 AD: R37G07 DBD	0	0	0	2	1	1	0	0	0	0	1	0	1	0	0	0	0	2	0	0	3	2	0	0
VT061711 AD: VT045603 DBD	4	0	5	2	0	0	0	3	0	0	3	6	3	2	0	2	0	3	8	2	4	3	3	3
R93D09 AD: VT038115 DBD	0	0	0	2	2	0	0	0	0	0	0	0	2	0	0	0	0	0	0	2	0	0	0	0
VT038115 AD: VT040055 DBD	0	0	0	2	0	3	0	0	0	0	N/A	N/A	N/A	N/A	N/A	N/A	N/A	N/A	N/A	N/A	N/A	N/A	N/A	N/A
VT0098323 AD: VT061711 DBD	1	0	0	2	0	2	0	2	0	0	N/A	N/A	N/A	N/A	N/A	N/A	N/A	N/A	N/A	N/A	N/A	N/A	N/A	N/A
VT0098323 AD: R20C06 DBD	0	0	0	0	0	2	0	3	0	1	N/A	N/A	N/A	N/A	N/A	N/A	N/A	N/A	N/A	N/A	N/A	N/A	N/A	N/A
R39B11 AD: VT061711 DBD	0	0	0	3	0	2	0	2	0	3	N/A	N/A	N/A	N/A	N/A	N/A	N/A	N/A	N/A	N/A	N/A	N/A	N/A	N/A
R48A07 AD: VT040055 DBD	0	0	0	1	0	1	1	0	0	0	N/A	N/A	N/A	N/A	N/A	N/A	N/A	N/A	N/A	N/A	N/A	N/A	N/A	N/A
VT038115 AD: VT061711 DBD	0	0	0	2	0	2	0	0	0	0	N/A	N/A	N/A	N/A	N/A	N/A	N/A	N/A	N/A	N/A	N/A	N/A	N/A	N/A
VT0098323 AD: R94E06 DBD	1	0	0	0	0	0	0	0	0	1	N/A	N/A	N/A	N/A	N/A	N/A	N/A	N/A	N/A	N/A	N/A	N/A	N/A	N/A
R22D12 AD: VT061711 DBD	2	0	0	0	1	1	0	3	2	3	N/A	N/A	N/A	N/A	N/A	N/A	N/A	N/A	N/A	N/A	N/A	N/A	N/A	N/A
R22D12 AD: R94E06 DBD	2	0	4	0	1	0	0	0	0	1	N/A	N/A	N/A	N/A	N/A	N/A	N/A	N/A	N/A	N/A	N/A	N/A	N/A	N/A
VT038115 AD: R94E06 DBD	0	0	0	0	0	0	0	0	0	0	N/A	N/A	N/A	N/A	N/A	N/A	N/A	N/A	N/A	N/A	N/A	N/A	N/A	N/A
R48A07 AD: R22D12 DBD	4	0	0	0	3	0	0	0	0	0	N/A	N/A	N/A	N/A	N/A	N/A	N/A	N/A	N/A	N/A	N/A	N/A	N/A	N/A
R94E06 AD: VT040055 DBD	1	0	0	0	0	3	0	0	0	0	N/A	N/A	N/A	N/A	N/A	N/A	N/A	N/A	N/A	N/A	N/A	N/A	N/A	N/A

647  
648  
649  
650

**Table S1. Proprioceptor expression of split-GAL4 driver lines in the legs of *Drosophila melanogaster*.** The number of cells labeled by the screened split-GAL4 driver lines was determined by counting cells genetically expressing membrane bound GFP and a nuclear reporter (i.e. UAS-

651 mCD8GFP; Redstinger) using confocal imaging. Proprioceptors that did not have their expression checked received a “N/A”. The lack of a column  
 652 for a particular proprioceptive class indicates that either no expression was seen or that proprioceptor was not checked for expression. HP: hair plate;  
 653 CS: campaniform sensilla.

654

## 655 Video Legends

656

657 **Video 1. Calcium activity of CxHP8 neurons while the left front leg was moved passively and slowly using a 3-axis platform.**

658

659 **Video 2. Animation of hair plates on the front leg of a fly walking on a treadmill.** The fly and hair plates were rendered in Blender and based on  
 660 high resolution confocal images. Depicted are the three hair-plates located at the thorax-coxa joint (CxHP4: red; CxHP3: green; CHP8: blue) and  
 661 three at the coxa-trochanter joint (TrHP5: orange; TrHP7: purple; TrHP6: pink).

662

663 **Video 3. Calcium activity of CxHP8 neurons while a fly behaved on a spherical treadmill.**

664

665

## 666 Methods

667

### 668 Fly Husbandry and Genotypes

669

670 Experiments were performed on adult male flies, *Drosophila melanogaster*, between 2-5 days post-eclosion. Flies were  
 671 reared in a 25°C incubator with 14:10 light:dark cycle within vials filled with a standard cornmeal and molasses medium.

672 Genotypes used in experiments are listed in Table 1.

673

Stock Name	Genotype	Figure(s)	Stock Source
R48A07 AD: R20C06 DBD > mCD8GFP; Redstinger	w[1118]/yw, hs flp, UAS-mCD8-GFP; P{+t[7.7]w[=mC]=R48A07-p65.AD}attP40/ UAS- stingerRed; P{y[+t7.7]w[+mC]=R20C06- GAL4.DBD}attP2/+	1, S1	UAS-mCD8GFP; Redstinger was gifted from the Parrish lab, University of Washington and crossed with split-GAL4 gifted from Moon Lab, Yonsei University (Bloomington Stocks #69841 and #71070)
R48A07 AD: R20C06 DBD > pJFRC7-20XUAS-IVS- mCD8::GFP	w[1118]/w[*]; P{+t[7.7]w[=mC]=R48A07- p65.AD}attP40/+; P{y[+t7.7]w[+mC]=R20C06- GAL4.DBD}attP2/P{pJFRC7-020XUAS-IVS- mCD8::GFP}attP2	1, S1	20X UAS-mCD8::GFP was gifted from the Rubin lab and crossed with split-GAL4 gifted from Moon Lab, Yonsei University (Bloomington Stocks #69841 and #71070)
R48A07 AD: R20C06 DBD > GcaMP7f; tdTomato	w[1118]/+ DL; P{+t[7.7]w[=mC]=R48A07- p65.AD}attP40/ P{w[+mC]= UAS-tdTom.S}2; P{y[+t7.7]w[+mC]=R20C06-GAL4.DBD}attP2/ PBac{y[+mDint2]w[+mC]=20xUAS-IVS- jGCaMP7f}VK00005	1, S1	UAS-GCaMP7f; tdTomato were contrasted from Bloomington stocks #36327 and #79031, and crossed with split- GAL4 gifted from Moon Lab, Yonsei University (Bloomington Stocks #69841 and #71070)
R48A07 AD: R20C06 DBD > ChrimsonR (CxHP8 optogenetic activation)	w[1118]/+ DL; P{+t[7.7]w[=mC]=R48A07- p65.AD}attP40/+ DL; P{y[+t7.7]w[+mC]=R20C06- GAL4.DBD}attP2/10X UAS ChrimsonR mCherry (attp2)/TM3 Sb	3, S3	UAS-ChrimsonR was gifted from Janelia (outcrossing was done by Anne Suster, University of Washington) and crossed with split-GAL4 gifted from Moon Lab, Yonsei University (Bloomington Stocks #69841 and #71070)

R48A07 AD: R20C06 DBD > GtACR1 (CxHP8 optogenetic silencing)	w[1118]/+ DL; P{+t[7.7]w[=mC]=R48A07-p65.AD}attP40/+ DL; P{y[+t7.7]w[+mC]=R20C06-GAL4.DBD}attP2/20X-UAS-GtACR1-EYFP (III) attp2	3, S3	UAS-GtACR1 stock was created by Anne Sustar in the Tuthill Lab at the University of Washington and was crossed with split-GAL4 gifted from Moon Lab, Yonsei University (Bloomington Stocks #69841 and #71070)
R52A01 DBD > GtACR1 (light-effect control)	w[1118]/+ DL; +/+ DL; P{y[+t7.7]w[+mC]=R52A01-GAL4.DBD}attP2/20X-UAS-GtACR1-EYFP (III) attp2	S3	UAS-GtACR1 stock was created by Anne Sustar in the Tuthill Lab at the University of Washington and was crossed with Bloomington Stock #69141
R48A07 AD: R20C06 DBD > Kir 2.1 (CxHP8 chronic silencing)	w[1118]/+ DL; P{+t[7.7]w[=mC]=R48A07-p65.AD}attP40/+ DL; P{y[+t7.7]w[+mC]=R20C06-GAL4.DBD}attP2/pJFRC49-10XUAS-IVS-eGFP::Kir2.1(attP2)	4, S4	Crossed Dickinson Lab Stock U-111 with split-GAL4 gifted from Moon Lab, Yonsei University (Bloomington Stocks #69841 and #71070)
R48A07 AD > Kir 2.1 (Control)	w[1118]/+ DL; P{+t[7.7]w[=mC]=R48A07-p65.AD}attP40/+ DL; pJFRC49-10XUAS-IVS-eGFP::Kir2.1(attP2)/+	4, S4	Crossed Dickinson Lab Stock U-111 with Bloomington Stock #71070
R39B11 AD > Kir 2.1 (Control)	w[1118]/+ DL; P{+t[7.7]w[=mC]=R39B11-p65.AD}attP40/+ DL; pJFRC49-10XUAS-IVS-eGFP::Kir2.1(attP2)/+	4, S4	Crossed Dickinson Lab Stock U-111 with Bloomington Stock #71040

674

675 **Table 1. *Drosophila melanogaster* genotypes used for experiments.**

676

677 **Blender Model of *Drosophila* Body and Front Leg Hair Plates**

678

679 A morphologically accurate model of an adult *Drosophila melanogaster* containing the hair plates at the thorax-coxa and  
680 coxa-trochanter joints of the front leg was constructed using the 3D rendering and modeling software, Blender (Vaxenburg  
681 et al., 2024). The body of the fly, and the anatomy and location of hair plates in the model were based on high-resolution  
682 confocal images. We replayed the 3D walking kinematics of the left front leg coxa measured from a tethered fly walking  
683 on the ball to this model to illustrate the phases during the step cycle when the hairs of each coxa hair plate would be  
684 deflected (**Video 2**).

685

686 **Confocal Imaging of Proprioceptor Expression**

687

688 *Peripheral expression of proprioceptors in legs*

689

690 Front, middle, and/or hind legs of male flies associated with the driver lines in **Table S1** crossed with the UAS-mcD8GFP;  
691 redstinger reporter line were fixed in a 4% formaldehyde (PFA) PBS solution for 20 minutes and then washed three times  
692 in a 0.2% Triton X-100 PBS solution. Legs were then cleared with FocusClear (CelExplorer) and mounted on slides in  
693 MountClear (CelExplorer). The expression at each hair plate was assessed using an Olympus FV1000 confocal  
694 microscope. The number of proprioceptor cells labeled by each driver line was then determined through visual inspection  
695 of the volumetric imaging stacks in FIJI (Schindelin et al., 2012)

696

697

698

699

## 700 *Central expression of proprioceptors in the brain and VNC*

701

702 The brain and VNC were dissected from male flies associated with the split-GAL4 driver lines that showed interesting  
703 peripheral expression in hair plates, such as the CxHP8 split-GAL4 driver line (i.e. R48A07 AD; R20C06 DBD). Unlike  
704 above, the GAL4 driver resulted in the expression of pJFRC7-20XUAS-IVS-mCD8::GFP. The brains and VNCs were  
705 fixed in the same manner as legs but then were put into a blocking solution (5% goat serum, PBS, 0.2% Triton-X) for 20  
706 minutes, followed by being incubated in a blocking and primary antibody solution (1:50 concentration of anti-GFP chicken  
707 antibody, 1:50 concentration of anti-brp mouse) for 24 hours at room temperature. The brains and VNCs were then washed  
708 three times in PBS with 0.2% Triton-X and incubated in a blocking and secondary antibody solution (1:250 concentration  
709 of anti-chicken-Alexa 488, 1:250 concentration of anti-mouse-Alexa 633). After this, the brains and VNCs were washed  
710 three times with PBST and mounted on a slide in Vectashield (Vector Laboratories). The brains and VNCs were imaged  
711 with the same Olympus confocal microscope as legs and image stacks were analyzed in FIJI (Schindelin et al., 2012).

712

## 713 **Reconstruction and Identification of Hair Plate Axons in FANC EM dataset**

714

### 715 *Hair Plate Axon Reconstruction and Connectivity*

716

717 Hair plate axons were reconstructed in the electron microscopy dataset of the female ventral nerve cord, FANC (Azevedo  
718 et al., 2024; Phelps et al., 2021), through manual proofreading of the automatically segmented cell fragments in  
719 Neuroglancer (Maitin-Shepard et al., 2021). Annotations containing information about the reconstructed hair plate axons,  
720 such as what hair plate they project from, we uploaded to the Connectome Annotation Versioning Engine (CAVE) and  
721 are publicly available to those that have access to the FANC dataset. We then determined and proofread the cell fragments  
722 that received or provided at least 3 synapses from or onto hair plate axons. In addition to proofreading the upstream and  
723 downstream partners of hair plates, we classified them, if possible, into general cell types and specific cell classes using  
724 pre-existing CAVE annotation tables and/or expert knowledge (Azevedo et al., 2024; Harris et al., 2015; Lacin et al.,  
725 2019; Lesser et al., 2024). The annotations of these neurons were also uploaded to CAVE and are publicly available. We  
726 determined the downstream and upstream partners of hair plates and performed connectivity analyses using a custom  
727 Python script. Note that only neurons that had 4 or more output synapses on average per neuron within a cell class onto  
728 individual downstream neurons were used in the reflex circuit analyses.

729

### 730 *Hair Plate Identification*

731

732 Hair axons were identified from previously traced backbones and annotations in CATMAID (Kuan et al., 2020; Phelps et  
733 al., 2021). The axons of CxHP8, CxHP3, and CxHP4 were identified based on if they projected through the ventral  
734 prothoracic, dorsal prothoracic, or prothoracic accessory nerves, respectively (**Figure S5A**). All trochanter hair plate  
735 axons project through the prothoracic leg nerve (**Figure S5A**), so TrHP5, TrHP6, and TrHP7 neurons were instead  
736 identified based on their location in the nerve bundle, axonal morphology, and downstream connectivity with motor  
737 neurons (**Figure 5D**). TrHP6 axons were identified because they make distinct connections onto motor modules compared  
738 to TrHP5 and TrHP7 (**Figure 5D**). TrHP5 and TrHP7 axons could be differentiated because they enter the leg neuropil  
739 through the ProLN at different locations (**Figure S5A**).

740

### 741 *Motor Impact Score*

742

743 Motor impact score (Lee et al., 2024) was computed by first calculating the monosynaptic weight between a hair plate  
744 and motor module, which is the total number of synapses that all neurons within a hair plate make onto the motor neurons  
745 within a motor module, divided by the total number of synapses onto that motor module across all neurons. Next, we

746 calculated the di-synaptic weight between a hair plate and motor module by finding and summing the proportion of hair  
747 plate input synapses provided to each premotor neuron connected to the motor module of interest, multiplied by the  
748 proportion of input synapses those premotor neurons make onto the motor module. Note that the fractional input between  
749 these premotor neurons and the motor module is signed, based on the hemilineages of the premotor neurons. The motor  
750 impact score is then derived by summing the monosynaptic and di-synaptic weights.

751

## 752 **Calcium Imaging of Hair Plate Axons**

753

754 We used a previously described preparation, setup, and analysis pipeline (Dallmann et al., 2023) to image calcium signals  
755 in hair plate axons in the neuromere of the left front leg during active and passive leg movements.

756

### 757 *Preparation*

758 We attached a fly to a custom-made holder, removed a rectangular piece of cuticle from the dorsal thorax, removed the  
759 underlying indirect flight muscles, and used an insect pin to displace the digestive system. This provided a dorsal view on  
760 the hair plate axons entering the VNC from the left front leg.

761

### 762 *Two-photon image acquisition*

763 Calcium signals in hair plate axons were recorded with a two-photon Movable Objective Microscope (MOM; Sutter  
764 Instruments) with a 20x water-immersion objective (Olympus XLUMPlanFI, 0.95 NA, 2.0 mm wd; Olympus). Hair plate  
765 neurons expressed the calcium indicator GCaMP7f (green fluorescence) and the structural marker tdTomato (red  
766 fluorescence). Fluorophores were excited at 920 nm by a mode-locked Ti:sapphire laser (Chameleon Vision S; Coherent).  
767 We used a Pockels cell to keep the power at the back aperture of the objective below ~35 mW. Emitted fluorescence was  
768 directed to two high-sensitivity GaAsP photomultiplier tubes (Hamamatsu Photonics) through a 705 nm edge dichroic  
769 beamsplitter followed by a 580 nm edge image-splitting dichroic beamsplitter (Semrock). Fluorescence was band-passed  
770 filtered by either a 525/50 (green) or 641/75 (red) emission filter (Semrock). Image acquisition was controlled with  
771 ScanImage 5.2 (Vidrio Technologies) in Matlab (MathWorks). The microscope was equipped with a galvo-resonant  
772 scanner, and the objective was mounted onto a piezo actuator (Physik Instrumente; digital piezo controller E-709). We  
773 acquired volumes of three 512 x 512 pixel images spaced 5  $\mu\text{m}$  apart in depth (10  $\mu\text{m}$  total) at a speed of 8.26 volumes  
774 per second.

775

### 776 *Two-photon image analysis*

777 Two-photon images were smoothed with a Gaussian filter (sigma = 3 pixels; size = 5 x 5 pixels). Each tdTomato image  
778 was aligned to the average tdTomato signal of the recorded trial using a cross-correlation-based image registration  
779 algorithm (Guizar-Sicairos et al., 2008). The same alignment was used for the GCaMP images. We averaged the three  
780 GCaMP and tdTomato images per volume. Then, we extracted the mean fluorescence in manually drawn regions of  
781 interest (ROIs). To correct for vertical movement of the VNC, we computed the ratio of GCaMP fluorescence to tdTomato  
782 fluorescence in each frame. To facilitate comparisons across trials and flies, ratio values were z-scored by subtracting the  
783 mean of a baseline ratio and dividing by the standard deviation of that baseline ratio. The baseline was defined in each  
784 trial as the 10% smallest ratio values. Finally, z-scored ratio values were upsampled to the sampling rate of leg tracking  
785 (300 Hz) using cubic spline interpolation and then low-pass filtered using a moving average filter with a time window of  
786 0.2 s.

787

### 788 *Platform and treadmill*

789 The platform consisted of a metal pin (0.5 mm diameter, 4.4 mm length) mounted onto a three-axis micromanipulator  
790 (MP-225; Sutter Instruments). The pin was wrapped in black sandpaper to provide sufficient grip for the flies' tarsi. The  
791 micromanipulator was controlled manually.

792

793 The treadmill consisted of a patterned Styrofoam ball (9.1 mm diameter; 0.12 g) floating on air in an aluminum holder.  
794 The air flow was set to ~500 ml/min. The ball was illuminated by two infrared LEDs (850-nm peak wavelength; ThorLabs)  
795 via optical fibers. Ball movements were recorded at 30 Hz with a camera (Basler acA1300-200um; Basler AG) equipped  
796 with a macro zoom lens (Computar MLM3X-MP; Edmund Optics). Ball rotations around the fly's cardinal body axes  
797 (forward, rotational, sideward) were reconstructed offline using FicTrac(Moore et al., 2014). Rotational velocities of the  
798 fly were calculated based on the known diameter of the ball. Velocities were upsampled to the sampling rate of leg tracking  
799 (300 Hz) using cubic spline interpolation and low-pass filtered using a moving average filter with a time window of 0.2  
800 s.

801

#### 802 *Leg tracking*

803 Movement of the left front leg was recorded at 300 Hz with two cameras (Basler acA800-510um; Basler AG) equipped  
804 with 1.0x InfiniStix lenses (68 mm wd; Infinity) and 875 nm short pass filters (Edmund Optics). The leg was illuminated  
805 by an infrared LED (850-nm peak wavelength; ThorLabs) via an optical fiber. We used a previously trained (Dallmann  
806 et al., 2023) deep neural network (Mathis et al., 2018) to automatically track all leg joints in each camera view. 2D tracking  
807 data from both camera views were then combined to reconstruct leg joint positions and angles in 3D using Anipose  
808 (Karashchuk et al., 2021).

809

#### 810 *Behavior classification*

811 Fly behavior was classified semi-automatically based on thresholds on the velocity of the front and middle leg tarsi as  
812 described previously (Dallmann et al., 2023). Flies on the platform were classified as resting or actively moving. Flies on  
813 the treadmill were classified as resting, walking, or grooming. All classifications were reviewed and manually corrected  
814 if necessary.

815

#### 816 *Data selection*

817 Frames were manually excluded from the analysis if the front leg was involved in movements other than walking or  
818 grooming on the treadmill (e.g., extended downward pushing), the femur-tibia joint of the front leg was not tracked  
819 correctly, or the two-photon image registration failed (e.g., the VNC moved out of the imaging volume).

820

### 821 **Optogenetic Activation and Silencing Experiments**

822

823 Optogenetic experiments were performed on adult male flies that were raised on 35mM in 95% EtOH ATR for 1-3 days,  
824 were 2-5 days old, de-winged, and fixed to a rigid tether (0.1 mm thin tungsten rod) with UV glue (KOA 300). These flies  
825 were placed onto a spherical foam ball (weight: 0.13 g; diameter: 9.08mm) suspended by air within a visual arena. A dark  
826 bar with a width of 30 degrees with respect to the fly oscillated at 2.7 Hz in front of the fly. A spatially precise red (638  
827 nm; 1200 Hz pulse rate; 30% duty cycle, Laserland) or green (532 nm; 1200 Hz pulse rate; 60% duty cycle, Laserland)  
828 laser was then positioned on the thorax-coxa joint of the left front leg. Optogenetic activation experiments were conducted  
829 on flies in which their CxHP8 neurons expressed ChrimsonR, whereas silencing experiments were performed on those  
830 that expressed GtACR1 in those neurons (**Table 1**). Trials were 2 seconds in duration and consisted of turning the laser  
831 on (experimental trials) or keeping it off (control trials) 0.5 seconds into the trial for 1 second. During each trial, the  
832 behavior each fly was recorded with 6 high-speed cameras (300 fps; Basler acA800-510  $\mu$ m; Basler AG) and the  
833 movement of the ball was recorded at 30 fps with a camera (FMVU-03MTM-CS) and processed using FicTrac (Moore et al.  
834 et al., 2014). The 3D positions of each leg joint and the corresponding joint angles were determined by using DeepLabCut  
835 (Mathis et al., 2018) and Anipose (Karashchuk et al., 2021). Kinematic analyses were performed in a custom Python  
836 script. Behaviors were classified using a previously published random forest classifier (Karashchuk et al., 2021). In  
837 addition, front leg grooming was also classified based on the proximity and velocity of the front legs.

838

## 839 **Treadmill Experiments**

840

841 Treadmill experiments were performed on 2-5 day old CxHP8 silenced and genetically-matched control male flies (**Table**  
842 **1**) using a previously described treadmill system and experimental protocol (Pratt et al., 2024). The inward rectifying  
843 potassium channel, Kir 2.1, was used to silence the activity of CxHP8 neurons throughout development. In short, trials  
844 consisted of placing a de-winged fly into a chamber and moving the belts of the split-belt treadmill at a steady-state speed  
845 of 10 mm/s for 20 minutes in total. During which, we recorded the behavior of the fly at 200 fps and in 20 second bouts  
846 with 5 high-speed cameras (Basler acA800-510  $\mu\text{m}$ ; Basler AG). We then used DeepLabCut (Mathis et al., 2018) and  
847 Anipose (Karashchuk et al., 2021) to reconstruct the 3D positions of head, thorax, abdomen, and each leg tip. Custom  
848 Python scripts were used to analyze and visualize walking kinematics and posture.

849

## 850 **Kinematic Classification and Parameters**

851

852 The classification and quantification of behavior, swing and stance, and most walking kinematic parameters for tethered  
853 flies and flies walking on the treadmill were conducted in the same manner as a prior study (Pratt et al., 2024). For tethered  
854 flies in both the calcium imaging and optogenetic experiments, steps or frames were classified as forward walking if the  
855 instantaneous forward velocity and absolute rotational velocity of the ball was greater than 5 mm/s and less than 25  
856 degrees/s, respectively. Left and right turns were classified as periods where the rotational velocity was less than -25  
857 degrees/s or greater than 25 degrees/s, respectively. Other behaviors, like rest/sanding and front leg grooming, were  
858 determined by using a previously published behavioral classifier (Karashchuk et al., 2021). For flies walking on the  
859 treadmill, forward walking was classified as periods where the body velocity had a forward velocity greater than 5 mm/s  
860 and the absolute heading angle with respect to the front of the chamber was less than 15 degrees. Rest periods are classified  
861 as those where the instantaneous velocity of the body and all tarsi was less than 5 mm/s (i.e. all legs in stance).

862

863 During walking, the classification of each leg into swing and stance was based on the smoothed (i.e. with a Gaussian  
864 Kernel) instantaneous velocity of the tarsus of each leg. Instantaneous values were negative during periods where the  
865 tarsus moved posteriorly along the longitudinal axis of the body. A leg was classified as being in swing if its tarsus had  
866 an instantaneous velocity greater than 5 mm/s or less than -25 mm/s. Otherwise, the leg was classified as being in stance.  
867 Short, 1 video frame, classifications of swing or stance were corrected and reclassified as the other phase of the step cycle.

868

869 Classified forward walking steps were further filtered to remove steps that occurred during the transition into forward  
870 walking or produced kinematics that were inconsistent with what was previously published (DeAngelis et al., 2019;  
871 Mendes et al., 2013; Strauss and Heisenberg, 1990; Wosnitza et al., 2013). Any step that didn't meet the following criteria  
872 for a forward walking step was removed: step frequency between 5 and 20 steps/s, a swing duration between 15 and 75  
873 ms, and a stance duration less than 200 ms. Steps that passed these filtering criteria were used for further kinematic  
874 analyses and comparisons.

875

876 All kinematic analyses and visualizations were done in custom Python scripts, which a publicly available on GitHub  
877 ([https://github.com/Prattbuw/Hair\\_Plate\\_Paper](https://github.com/Prattbuw/Hair_Plate_Paper)).

878

## 879 **Statistical Analyses**

880

881 Bootstrapping or t-tests were performed to determine statistical significance. If multiple comparisons were performed, a  
882 Bonferroni correction was employed to adjust the threshold of significance. t-tests were used to compare posture and step

883 kinematics between CxHP8 silenced and control flies, along with joint angle distributions and tarsus positions during  
884 behavior. A Kuiper two-sample was used to assess statistical significance for inter-leg coordination. Finally, bootstrapping  
885 was used to statistically compare the anterior and posterior extreme positions between these flies.

886

## 887 **Glossary of Kinematic Parameters**

888

889 **Body length (BL):** the distance between the head and distal part of the abdomen.

890

891 **Body height:** the vertical distance between the ground and thorax.

892

893 **Body angle:** the angle made by the body frame.

894

895 **Anterior extreme position:** the position where a leg first contacts the ground (i.e. stance onset) in egocentric coordinates.

896

897 **Posterior extreme position:** the position where a leg first takes off from the ground (i.e. swing onset) in egocentric  
898 coordinates.

899

900 **Swing distance:** the total lateral and longitudinal distance a leg travels during the swing phase of the step cycle.

901

902 **Swing duration:** the duration of the aerial phase of leg movement during walking.

903

904 **L1 relative phase:** the relative offset in the stance onsets between the left front leg and the leg of interest with respect to  
905 the left front leg's step cycle.

906

907 **Polygon area:** The area in  $BL^2$  of the polygon formed by the tarsi tip positions of the legs in stance.